University of Twente
Applied Mathematics; Mathematics of Computational Science

Least-Squares Finite Element Method for the Fluid-Structure Interaction Spectral Problem

Carmen Tretmans

Supervisor:
dr. F.H.C. Bertrand

Graduation Committee:
dr. F.H.C. Bertrand
dr. M. Schlottbom
dr. rer. nat. J.A. Iglesias Martínez

March 2023

Abstract

A least-squares finite element method (LSFEM) for the fluid-structure interaction problem is derived. The fluid-structure interaction problems deals with the vibration caused by an elastic structure in contact with a fluid. The fluid-structure interaction is treated as a first-order system, after which the least-squares functional is formulated using L^2-norm residuals. Norm-equivalence of the least-squares functional is proven which ensures the favorable properties of the Rayleigh-Ritz setting. As a result, a priori error estimates are obtained for the LSFEM approximation. Furthermore, we highlight steps taken towards numerical implementation and demonstrate convergence for a simplified test case. Finally, the least-squares functional is used as an inherent a posteriori error estimate for a primal displacement/pressure formulation.

Acknowledgement

This thesis would not have been written without the support of many people. I would like to thank Fleurianne Bertrand for supervising this project. Furthermore, I wish to thank the additional members of my graduation committee, Matthias Schlottbom and José Iglesias, for taking the time and the effort to read and review my work.

Met het schrijven van deze laatste woorden van mijn masterscriptie sluit ik niet alleen mijn master af, maar ook mijn studententijd in Enschede. Na acht jaar student te zijn geweest in Enschede zijn er heel wat mensen die ik wil bedanken.

Allereerst wil ik natuurlijk mijn ouders, Melina en Leander bedanken voor alle steun die zij hebben geboden. Verder grote dank aan mijn grootouders voor alle hulp en voedselpakketten. Niet te vergeten, Huize Poolside. Zonder jullie had ik me nooit zo thuis gevoeld in Enschede. Wilja, voor alle reisjes naar Parijs, en al mijn overige (wiskunde)vriendjes met wie ik soms wel, soms ook geen, studiepunten heb behaald. En natuurlijk Sagy, voor de kopjes koffie wanneer ze broodnodig waren.

Contents

1 Introduction

1.1 Background

One of the most powerful methods for the numerical approximation of partial differential equations is the finite element method (*FEM*). It is widely used in engineering, due to its easy implementations, easy geometrical adjustments and numerical stability. Mathematically, it relies on a well-founded theory for a vast majority of problems, making it an overall beloved method. One of the reasons finite element methods work so well is the strong link between differential equations and variational principles. A key result in finite element methods is the so-called Rayleigh-Ritz principle, stating that FEM provides significant computational and analytical advantages if the variational foundation is provided by a convex quadratic functional. This is why the finite element method is found to work well for problems with an underlying unconstrained, quadratic energy minimization principle. These are found in, for example, structural analysis, incompressible fluid flows or electromagnetics.
For problems without the advantageous Rayleigh-Ritz setting, efficient finite element methods are often less straightforward and require an adjusted mathematical framework. For a long time FEM has not been applied to those kind of problems. However, due to the powerful performance of FEM, the wish arose to extend FEM to these problems. At this point the Least-Squares Finite Element Method (*LSFEM*) was introduced. The main idea behind LSFEM is to reformulate the problem to a setting that falls into the Rayleigh-Ritz principle. Whereas for traditional FEM the variational problem is imposed by the partial differential equation, for LSFEM the variational problem is externally dictated based on the equations residual. The equations residual is captured in a least-squares functional which gives rise to the name *Least-squares finite element method*. Using this strategy, almost all advantages of the Rayleigh-Ritz setting can be recovered, see for example [15].

1.2 Problem Statement

In this thesis we will approximate the free vibration modes of an elastic structure in contact with an incompressible fluid using a least-squares finite element method. The fluid-structure interaction plays an important role in many engineering fields and has therefore been studied extensively, see for example [12] or [22] for an overview. Free vibration modes occur when the system is allowed to vibrate freely. Mathematically, the free vibration modes translate to the eigenvalues of an underlying eigenvalue problem. The aim of this thesis is to formulate the underlying eigenvalue problem using an LSFEM approach. The main result will be the norm-equivalence of the LS functional, resulting in existence and uniqueness of the solution. The eigenvalueproblem is then numerically solved.

1.3 A Standard Finite Element Setup and the Rayleigh-Ritz Setting

Originally, FEM was constructed as a weighted residual method, like the Galerkin method. The finite element approximation is chosen to satisfy the PDE in a weak sense where the PDE is integrated against a set of weighting functions. Consider a general boundary value problem on the bounded domain $\Omega \subset \mathbb{R}^d$ with boundary Γ. The aim is to find $u \in \mathcal{U}$ such

that

$$\mathcal{L}u = f \text{ in } \Omega \ ,$$
$$\mathcal{R}u = g \text{ on } \Gamma \ .$$

Here we assume that $\mathcal{L}$ is a linear differential operator, $\mathcal{R}$ the boundary operator and $\mathcal{U}$ the desired solution space. The standard finite element approach is to multiply the solution $u \in \mathcal{U}$ by a test function $v \in \mathcal{V}$ in a suitable space $\mathcal{V}$ and integrate over the domain. Essential boundary conditions are imposed on the solution space $\mathcal{U}_g = \{u \in \mathcal{U} \mid \mathcal{R}u|_\Gamma = g\}$, natural boundary conditions are naturally derived from the system. After multiplication by the test function, one obtains the weak form of the problem, of which the aim is to find $u \in \mathcal{U}_g$ such that

$$a(u, v) = l(v) \quad \forall v \in \mathcal{V} \ , \tag{1}$$

with the bilinear and linear forms

$$a(u, v) = \langle \mathcal{L}u, v \rangle \quad \text{and} \quad l(v) = \langle f, v \rangle \ .$$

To discretize the system the domain is partitioned into elements and the solution space $\mathcal{U}_g$ is approximated by the finite element space $\mathcal{U}_g^h$ on each element. The finite element space is spanned by a set of basis functions ϕ_i, $0 \leq i \leq N$. Approximating the unknown u in $\mathcal{U}_g^h$ leads to the finite element solution

$$u_h(\boldsymbol{x}) = \sum_i u_i \phi_i(\boldsymbol{x}) \ .$$

The choice of finite element space and basis functions is not unique, but affects the computability of the problem. A convenient choice are basis functions that are zero on most elements, creating a sparse system. After stating the discrete weak formulation

$$a(u_h, v) = l(v) \quad \forall v \in \mathcal{V} \ ,$$

and choosing suitable test functions $v \in \mathcal{V}$, we obtain a discrete system of the form

$$\boldsymbol{A}\vec{u} = \vec{f} \ ,$$

which can now be solved in terms of the coefficients $\vec{u}$. The entries of the matrix $\boldsymbol{A}$ and vector $\vec{f}$ are determined by

$$\boldsymbol{A}_{ij} = \langle \phi_i, v_j \rangle \quad \text{and} \quad \vec{f}_j = \langle f, v_j \rangle$$

for some test function v_j.

An important result in terms of existence and uniqueness of the solution is the Rayleigh-Ritz principle, linking the problem to a convex minimization problem, [15, Proposition 1.6]. Fundamental for the Rayleigh-Ritz setting is the coercivity, continuity, and symmetry of the bilinear form:

Definition 1.1 (Strong Coercivity)**.** The bilinear form $a(\cdot, \cdot)$ on $\mathcal{U} \times \mathcal{U}$ is strongly coercive if for some $\beta > 0$,

$$a(u, u) \geq \beta \|u\|_{\mathcal{U}}^2$$

holds for all $u \in \mathcal{U}$.

Definition 1.2 (Continuity)**.** The bilinear form $a(\cdot,\cdot)$ on $\mathcal{U}\times\mathcal{U}$ is continuous if for some $\alpha > 0$

$$|a(u,v)| \leq \alpha \|u\|_{\mathcal{U}} \|v\|_{\mathcal{U}}$$

holds for all $u, v \in \mathcal{U}$.

Definition 1.3 (Symmetry)**.** The bilinear form $a(\cdot,\cdot)$ on $\mathcal{U}\times\mathcal{U}$ is symmetric if for any $u, v \in \mathcal{U}$

$$a(u,v) = a(v,u) \ .$$

The Rayleigh-Ritz setting then reads:

Theorem 1.1 (Rayleigh-Ritz principle)**.** *Let $l(v)$ denote a bounded linear functional on $\mathcal{U}$ and $a(\cdot,\cdot)$ denote a continuous, strongly coercive and symmetric bilinear form on $\mathcal{U}\times\mathcal{U}$. Then, the problem* (1) *is equivalent to the unconstrained optimization problem: Find $u \in \mathcal{U}_g$ that minimizes*

$$J(u,f) = \frac{1}{2}a(u,u) - l(u) \ .$$

Indeed, the weak formulation (1) is the first order necessary condition that solutions u of the unconstrained minimization problem must satisfy. It is straightforward to check that the functional $J(\cdot,f)$ is convex and hence admits a unique solution to the minimization problem. In fact, the restrictions made to the bilinear form are identical to the ones made in the better-known Lax-Milgram Lemma, see e.g. [10, Chapter 4.1; Theorem 4.1.6], which ensures existence and uniqueness for the weak formulation. The Rayleigh-Ritz setting ensures that the finite element solution $u^h \in \mathcal{U}_g^h$ is a true projection of $u \in \mathcal{U}_g$ with respect to the inner product $a(\cdot,\cdot)$ and that the error $u_h - u$ is orthogonal to all elements in the approximating space,

$$\begin{aligned} a(u^h, v^h) &= a(u, v^h) \quad \forall v^h \in \mathcal{U}_g^h \ , \\ a(u^h - u, v^h) &= 0 \quad \forall v^h \in \mathcal{U}_g^h \ . \end{aligned}$$

1.4 Introducing the Least-Squares Finite Element Method

For problems that do not satisfy the Rayleigh-Ritz setting a least-squares finite element method can be constructed. Here we introduce the core ideas of this approach, as described in, for example, [15]. We consider the same problem, namely to find $u \in \mathcal{U}$ such that

$$\begin{aligned} \mathcal{L}u &= f \text{ in } \Omega \ , \\ \mathcal{R}u &= g \text{ on } \Gamma \ . \end{aligned} \tag{2}$$

Instead of formulating the variational form by taking the inner-product with a test function, the least-squares method is built on the equations residual,

$$J(u; f, g) = \|\mathcal{L}u - f\|_{H_\Omega}^2 + \|\mathcal{R}u - g\|_{H_\Gamma}^2 \ .$$

Here, the data spaces are denoted by H_Ω and H_Γ for the domain and boundary, respectively. Although the boundary conditions can be incorporated into the solution space in some cases, adding auxiliary terms to the least-squares formulation might be beneficial due

to its straightforward way to impose more complex boundary conditions. The variational problem is then defined as the minimization of the least-squares functional,

$$\min_{u \in \mathcal{U}} J(u; f, g) \ . \tag{3}$$

As a consequence of the first order necessary condition,

$$\frac{d}{d\theta} J(u + \theta v; f, g)|_{\theta=0} = 0 \quad \forall v \in \mathcal{U} \ ,$$

the weak formulations reads as follows: Find $u \in \mathcal{U}$ such that

$$(\mathcal{L}v, \mathcal{L}u)_{H_\Omega} + (\mathcal{R}v, \mathcal{R}u)_{H_\Gamma} = (\mathcal{L}v, f)_{H_\Omega} + (\mathcal{R}v, g)_{H_\Gamma} \quad \forall v \in \mathcal{U} \ .$$

More compactly, the problem can be reformulated to

$$a(u, v) = l(v) \ \forall v \in \mathcal{U} \ , \tag{4}$$

where we define the bilinear form

$$a(u, v) = (\mathcal{L}v, \mathcal{L}u)_{H_\Omega} + (\mathcal{R}v, \mathcal{R}u)_{H_\Gamma} \quad \forall u, v \in \mathcal{U} \tag{5}$$

and the linear form

$$l(v) = (\mathcal{L}v, f)_{H_\Omega} + (\mathcal{R}v, g)_{H_\Gamma} \quad \forall v \in \mathcal{U} \ . \tag{6}$$

An LSFEM can now be constructed by restricting the minimization problem to a finite element subspace $\mathcal{U}^h$,

$$\min_{u^h \in \mathcal{U}^h} J(u^h; f, g) \ , \tag{7}$$

with subsequent variational form: find $u^h \in \mathcal{U}^h$ such that

$$(\mathcal{L}v, \mathcal{L}u^h)_{H_\Omega} + (\mathcal{R}v, \mathcal{R}u^h)_{H_\Gamma} = (\mathcal{L}v, f)_{H_\Omega} + (\mathcal{R}v, g)_{H_\Gamma} \quad \forall v \in \mathcal{U}^h \ .$$

After choosing an appropriate basis for the finite element space this leads to a discrete system of the form

$$\boldsymbol{A}\vec{u} = \vec{f} \tag{8}$$

which can be solved for $\vec{u}$.

Key to the success of an LSFEM is the well-posedness of the underlying problem. Indeed, the well-posedness is a sufficient condition for recovering the desired Rayleigh-Ritz properties, see [15, Theorem 2.5],

Theorem 1.2 (LSFEM: Existence and Uniqueness)**.** *Assume the operator equation* (2) *to be well-posed, so that there exist positive constants* α_1, α_2 *such that*

$$\alpha_1 \|u\|^2_{\mathcal{U}} \leq \|\mathcal{L}u\|^2_{H_\Omega} + \|\mathcal{R}u\|^2_{H_\Gamma} \leq \alpha_2 \|u\|^2_{\mathcal{U}}$$

holds. Furthermore assume that $\mathcal{U}^h \subset \mathcal{U}$*. Then*

- *the bilinear form* (5) *is continuous, symmetric, and strongly coercive,*

- *the linear functional* (6) *is continuous,*
- *the variational formulation* (4) *has a unique solution* $u \in \mathcal{U}$ *that is also the unique solution of the minimization problem* (3)*,*
- *the discrete variation formulation* ($a(u^h, v) = l(v)\ \forall v \in \mathcal{U}^h$) *has a unique solution* $u^h \in \mathcal{U}^h$ *that is also the unique solution of the minimzation problem* (7)*,*
- *for some constant* $C > 0$*,* u *and* u^h *satisfy the error estimate*

$$\|u - u^h\|_{\mathcal{U}} \leq C \inf_{v^h \in \mathcal{U}^h} \|u - v^h\|_{\mathcal{U}} \ ,$$

- *the matrix* $\boldsymbol{A}$ *in equation* (8) *is symmetric and positive definite.*

Note that the restrictions made are less weighty as for the Rayleigh-Ritz setting as it is only necessary to impose the well-posedness of the problem for a conforming finite element space $\mathcal{U}^h \subset \mathcal{U}$. This is one of the key strengths of LSFEM compared to the classical finite element approach. It is also important to note that the well-posedness of the problem is equivalent to the norm equivalence of the residual functional, namely,

$$\alpha_1 \|u\|_{\mathcal{U}}^2 \leq \|\mathcal{L}u\|_{H_\Omega}^2 + \|\mathcal{R}u\|_{H_\Gamma}^2 \leq \alpha_2 \|u\|_{\mathcal{U}}^2 \quad \forall u \in \mathcal{U}$$

if and only if

$$\alpha_1 \|u\|_{\mathcal{U}}^2 \leq J(u;0;0) \leq \alpha_2 \|u\|_{\mathcal{U}}^2 \quad \forall u \in \mathcal{U} \ .$$

Making sure the least-squares functional is norm equivalent is hence of great importance when constructing an LSFEM. Proving norm equivalence of the LS functional of the fluid-structure interaction problem will be the main theoretical result of this thesis.

In addition to the beneficial Rayleigh-Ritz setting, LSFEM possesses an inherent error estimate, which is useful for adaptive mesh refinements. Moreover, the method constructs approximations to all variables in appropriate spaces simultaneously, simplifying the treatment of interface conditions arising in physical problems. Interface conditions can either be built directly into the solution spaces or be added as auxiliary terms to the least-squares functional. Additionally, the construction of symmetric, positive definite matrices is computationally advantageous for the discrete formulation.

Like any numerical method, LSFEM has its drawbacks, too. One can observe that LSFEM increases the order of the variational formulation. Hence, it is disadvantageous to apply LSFEM to higher order problems in a straightforward way. It is beneficial to reformulate a higher order systems to a first order system before applying LSFEM, to prevent a drastic increase in the order of the operator. Since this can often be done in multiple ways, LSFEM is not as straightforward in these cases. Furthermore, there are often multiple choices for data spaces and solution spaces yielding norm equivalence of the LS functional. One has to consider that the chosen spaces result in convenient discrete methods, for example in terms of easy construction of bases and norm evaluation.

1.5 State of the Art

Finite element methods have been deeply investigated since the 1950s and developed into a powerful tool for the numerical approximation of PDEs. Extensive research on LSFEM

however started much later. One reason for this was that FEM first was mainly applied to the field of structural analysis due to its good results. The underlying reason of this beneficial behavior, the connection with the minimization of an energy functional, was only discovered later. Only in In the 1990s, LSFEM became popular in the field of fluid dynamics, more particularly as a method of numerically approximating the Navier-Stokes equations, see Jiang [16] and Bochev and Gunzburger [7]. A fundamental work was published in 2009 by Gunzburger and Bochev [15], giving an extensive overview and theoretical foundation of LSFEM for various types of problems. Since then, it has become a popular tool in many different application areas due to its straightforward application to a vast majority of problems. It is widely used for problems with complex interface conditions, see for example the model of a Stokes-Darcy flow by Münzenmaier and Starke in [21]. In [6] a least-squares discretization for the simulation of blood flow in liver lobules is presented. An inherent error estimate and adaptive mesh refinements for first-order systems are analyzed in [3].
Relatively few papers deal with the eigenvalue problems associated with LSFEM. In [9] a first-order least-squares formulation for approximation of eigenvalues of Maxwells equation is presented. More recently, in [4] various formulations for the spectral Dirichlet Laplace problem are presented.
An LSFEM for the fluid-structure interaction has, to the knowledge of the author, not yet been developed. Kaiser-Herold and Matthies have analyzed the movements of an elastic beam and cylinder in a channel flow in [17] and [18]. However, this setup is different from the setting presented here. There are various approaches for approximating the eigenvalues of the fluid-structure interaction. Examples include the work of Bermúdez et al. [1] where several FEM formulations for the problem were developed as a follow-up of the model described by Bermúdez and Rodríguez in [2]. A model including an open surface of the structure is presented by Meddahi et al. [20] and Meddahi and Mora [19].

1.6 Outline

The structure of this thesis is as follows: Section 2 sketches the problem and introduces all necessary notations. Section 3 introduces the mesh and finite elements. The least-squares functional and corresponding weak formulation are derived in Section 4, with the main result presented in Section 4.3 resulting in existence and uniqueness of the solution. The section concludes with the construction of the finite element spaces, the discrete formulation and an a priori error estimate. Remarks on the implementation and numerical results of the method are presented in Section 5. These are followed by results of the least-squares functional as error estimate for the pressure/displacement formulation in Section 6. We conclude this thesis with an outlook in Section 7.

2 Governing Equations

We will introduce the notation for the used variables and function spaces in Section 2.1. In Section 2.2, we describe the physical domain and derive the governing equations of the fluid-structure interaction problem.

2.1 Notations

Assume $\Omega \subset \mathbb{R}^d$, $d = 2, 3$ is a bounded domain with Lipschitz boundary $partial\Omega$ with unit normal $\boldsymbol{\nu}$. In the following sections we will denote vectors $\boldsymbol{v} \in \mathbb{R}^d$ and matrices $\boldsymbol{\tau} \in \mathbb{R}^{d\times d}$ by bold symbols. Scalars are denoted by plain symbols. For $\boldsymbol{\tau} : \Omega \to \mathbb{R}^{d\times d}$ and $\boldsymbol{v} : \Omega \to \mathbb{R}^d$ we define the row-wise divergence, $\operatorname{div} \boldsymbol{\tau} : \Omega \to \mathbb{R}^d$, and the row-wise gradient, $\operatorname{grad} \boldsymbol{v} : \Omega \to \mathbb{R}^{d\times d}$, by

$$(\operatorname{div} \boldsymbol{\tau})_i \coloneqq \sum_j \partial_j \tau_{ij} \qquad \text{and} \qquad (\operatorname{grad} \boldsymbol{v})_{ij} \coloneqq \partial_j v_i \ .$$

The componentwise inner product of two matrices $\boldsymbol{\sigma}, \boldsymbol{\tau} \in \mathbb{R}^{d\times d}$ is denoted $\boldsymbol{\sigma} : \boldsymbol{\tau} \coloneqq tr(\boldsymbol{\tau}^T \boldsymbol{\sigma})$, where $tr(\boldsymbol{\tau}) \coloneqq \sum_{i=1}^d \tau_{ii}$ and $\boldsymbol{\tau}^T \coloneqq (\tau_{ji})$ represent the trace and the transpose of $\boldsymbol{\tau}$, respectively. Furthermore, we will use standard notation for Sobolev spaces. We define:

- The space of square-integrable functions,

$$L^2(\Omega) \coloneqq \{v : \ \Omega \to \mathbb{R} : \int_\Omega |v|^2 \ d\Omega < \infty\} \ .$$

  We use boldface to represent vector and tensor spaces, i.e.,

$$\boldsymbol{L}^2(\Omega) \coloneqq \{\boldsymbol{v} : \ \Omega \to \mathbb{R}^d : \int_\Omega |\boldsymbol{v} \cdot \boldsymbol{v}| \ d\Omega < \infty\} \ ,$$
$$\boldsymbol{L}^2(\Omega) \coloneqq \{\boldsymbol{\tau} : \ \Omega \to \mathbb{R}^{d\times d} : \int_\Omega |\boldsymbol{\tau} : \boldsymbol{\tau}| \ d\Omega < \infty\} \ ,$$

  respectively. The associated inner products are denoted by

$$\langle v, w\rangle_{L^2(\Omega)} = \int_\Omega vw \ d\Omega \ ,$$
$$\langle \boldsymbol{v}, \boldsymbol{w}\rangle_{L^2(\Omega)} = \int_\Omega \boldsymbol{v} \cdot \boldsymbol{w} \ d\Omega \ ,$$
$$\langle \boldsymbol{\tau}, \boldsymbol{\sigma}\rangle_{L^2(\Omega)} = \int_\Omega \boldsymbol{\tau} : \boldsymbol{\sigma} \ d\Omega \ .$$

  The associated norms are defined as $\|v\|_{L^2(\Omega)} = \left(\langle v, v\rangle_{L^2(\Omega)}\right)^{1/2}$.

- The space of functions in $L^2(\Omega)$ with weak derivatives in $L^2(\Omega)$,

$$H^1(\Omega) \coloneqq \{v \in L^2(\Omega) : \ \nabla v \in \boldsymbol{L}^2(\Omega)\}$$

  with the norm $\|v\|_{H^1(\Omega)} = \left(\|v\|^2_{L^2(\Omega)} + \|\nabla v\|^2_{L^2(\Omega)}\right)^{1/2}$.

- The space of functions in $H^1(\Omega)$ with vanishing trace on part of the boundary $\Gamma \subseteq \partial\Omega$,

$$H^1_\Gamma(\Omega) \coloneqq \{v \in H^1(\Omega) : v|_\Gamma = 0\} \ .$$

- The space of vector fields in $\boldsymbol{L^2}(\Omega)$ with divergence in $L^2(\Omega)$,

$$H(\mathrm{div};\Omega) \coloneqq \{\boldsymbol{v} \in \boldsymbol{L}^2(\Omega) : \ \mathrm{div}\ \boldsymbol{v} \in L^2(\Omega)\}$$

  endowed with the norm $\|\boldsymbol{v}\|_{H(div;\Omega)} = \left(\|\boldsymbol{v}\|^2_{L^2(\Omega)} + \|\mathrm{div}\ \boldsymbol{v}\|^2_{L^2(\Omega)}\right)^{1/2}$. Similarly we define the tensor space

$$\boldsymbol{H}(\mathrm{div};\Omega) \coloneqq \{\boldsymbol{\tau} \in \boldsymbol{L}^2(\Omega) : \ \mathrm{div}\ \boldsymbol{\tau} \in \boldsymbol{L}^2(\Omega)\} \ .$$

- The space of functions in $H(div;\Omega)$ with vanishing normal component on part of the boundary $\Gamma \subseteq \partial\Omega$,

$$H_\Gamma(div;\Omega) \coloneqq \{\boldsymbol{v} \in H(div;\Omega) : \boldsymbol{v}\cdot\boldsymbol{\nu}|_\Gamma = 0\} \ ,$$
$$\boldsymbol{H}_\Gamma(div;\Omega) \coloneqq \{\boldsymbol{\tau} \in \boldsymbol{H}(div;\Omega) : \boldsymbol{\tau}\boldsymbol{\nu}|_\Gamma = \boldsymbol{0}\} \ .$$

We furthermore recall:

- The trace space of $H^1(\Omega)$, assuming a Lipschitz continuous boundary $\partial\Omega$,

$$H^{1/2}(\partial\Omega) \coloneqq tr(H^1(\Omega)) = \{v \in L^2(\partial\Omega) \mid \exists\ u \in H^1(\Omega) : \ tr(u) = v\}$$

  with the associated norm

$$\|v\|_{H^{1/2}(\partial\Omega)} \coloneqq \inf_{\tilde{u}\in H^1(\Omega)} \{\|\tilde{u}\|_{H^1(\Omega)} \mid tr(\tilde{u}) = v\} \ .$$

Lastly, we define:

- The restricted spaces

$$\bar{H}(div;\Omega) = \{\boldsymbol{v} \in H(div;\Omega) : \ \boldsymbol{v}\cdot\boldsymbol{\nu} \in L^2(\Gamma)\} \ ,$$
$$\bar{\boldsymbol{H}}(div;\Omega) = \{\boldsymbol{\tau} \in \boldsymbol{H}(div;\Omega) : \ \boldsymbol{\tau}\boldsymbol{\nu} \in \boldsymbol{L}^2(\Gamma)\} \ ,$$

  for $\Gamma \subseteq \partial\Omega$. These spaces are introduced since traces of $H(div,\Omega)$ are in general not in $L^2(\partial\Omega)$. The space is endowed with the norm

$$\|\boldsymbol{v}\|_{\bar{H}(div;\Omega)} \coloneqq \left(\|\boldsymbol{v}\|^2_{H(div;\Omega)} + \|\boldsymbol{v}\cdot\boldsymbol{\nu}\|^2_{L^2(\Gamma)}\right)^{1/2} \ .$$

We furthermore introduce some additional notation: For matrices we denote the symmetric and skew-symmetric parts respectively by

$$sym(\boldsymbol{\tau}) = \frac{\boldsymbol{\tau} + \boldsymbol{\tau}^T}{2} \quad \text{and} \quad sk(\boldsymbol{\tau}) = \frac{\boldsymbol{\tau} - \boldsymbol{\tau}^T}{2} \ .$$

Finally, we denote the identity matrix by $\boldsymbol{\delta} \coloneqq \boldsymbol{\delta}_{d\times d}$ and define the skew-symmetric matrix $\boldsymbol{\chi}$ for the two-dimensional case as

$$\boldsymbol{\chi} = \begin{bmatrix} 0 & -1 \\ 1 & 0 \end{bmatrix} \ .$$

The definition for the three-dimensional case will be omitted for now due to later simplification to the two-dimensional case.

2.2 The Coupled System

In this section we introduce the elastoacoustic problem that will be studied. The elastoacoustic problem describes the motion of an elastic structure in contact with an incompressible fluid. We are specifically interested in the free vibration modes of the elastoacoustic problem. Examples of such a setup is, for example, a steel cavity filled with water.

In our setup, the domain Ω is split into two subdomains, Ω_S and Ω_F representing the solid and fluid domain, respectively. The solid domain will be governed by the equations of linear elasticity. The solid domain surrounds the fluid domain. It will be assumed that the boundaries of both domains, $\partial\Omega_S$ and $\partial\Omega_F$, are Lipschitz continuous. The interface of the two domains will be denoted by $\Sigma = \partial\Omega_S \cap \partial\Omega_F$, which will be orientated by the outward unit normal $\boldsymbol{\nu}_F$ of $\partial\Omega_F$. The remainder of the structure boundary $\partial\Omega_S \setminus \Sigma$ is the union of a Dirichlet part $\Gamma_D \subset \partial\Omega_S$ and a Neumann part $\Gamma_N \subset \partial\Omega_S$ describing the structure being fixed and free of stress, respectively. These boundary parts are oriented by the unit outward normal of $\partial\Omega_S$, denoted by $\boldsymbol{\nu}_S$. We furthermore assume $|\Gamma_D| \neq 0$ for simplicity later on. The boundary of the fluid domain consists entirely of the joint interface Σ. An example of this domain can be found in Figure 1.
We furthermore summarize the notation for later reference:

- Ω_S: structural domain,
- Ω_F: fluid domain,
- Γ_D: Dirichlet boundary of structure,
- Γ_N: Neumann boundary of structure,
- Σ: fluid-structure interface.

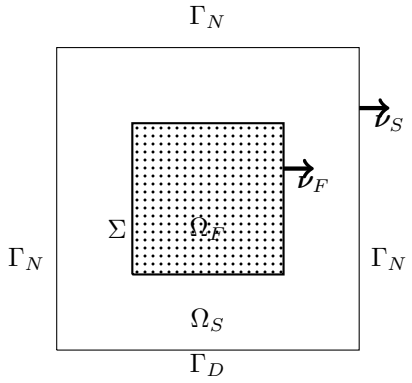

Figure 1: Example of fluid and solid domains.

To describe the physical model we make various simplifications and assumptions. Firstly, we consider homogeneous fluids with constant mass density. In addition, viscous and convective effects are assumed to be irrelevant due to small velocities. Lastly, we neglect gravity effects on the structure. As mentioned in the previous section, the least-squares methods requires a first order system. Throughout the derivation of the model, we will transform the governing equations to match the requirements of the least-squares method.

The following governing equations are mainly motivated by the systems described in [19], [20] and [5].

The deformation of the elastic structure is described in terms of its displacement vector $\boldsymbol{u} = \begin{bmatrix} u_x & u_y \end{bmatrix}^T$ and stress tensor $\boldsymbol{\sigma}$. In the case of small displacements, we can assume linear response of the structure. The constitutive equation for a linear elastic structure is governed by Hooke's Law, coupling the stress tensor $\boldsymbol{\sigma}$ with the linearized strain tensor $\epsilon(\boldsymbol{u}) \coloneqq \frac{1}{2}(\text{grad } \boldsymbol{u} + (\text{grad } \boldsymbol{u})^T)$,

$$\boldsymbol{\sigma} = \mathcal{C}\epsilon(\boldsymbol{u}) = \lambda \; tr(\epsilon(\boldsymbol{u})) \; \boldsymbol{\delta} + 2\mu \; \epsilon(\boldsymbol{u}) \; .$$

Here λ and μ are the positive Lamé coefficients. We have introduced the elasticity operator $\mathcal{C} : \mathbb{R}^{d\times d} \to \mathbb{R}^{d\times d}$ and observe that the operator preserves the symmetry of the linearized strain tensor. Furthermore, one can check that its inverse is given by

$$\mathcal{C}^{-1}\boldsymbol{\sigma} = \frac{1}{2\mu}(\boldsymbol{\sigma} - \frac{\lambda}{d\lambda + 2\mu} \; tr(\boldsymbol{\sigma}) \; \boldsymbol{\delta}) \; .$$

The equation of motion follows from Newton's second law,

$$\text{div } \boldsymbol{\sigma} = -\boldsymbol{f}_S \text{ in } \Omega_S \quad ,$$

with $\boldsymbol{f}_S$ describing an external force. The structure is fixed along the boundary part Γ_D and we impose

$$\boldsymbol{u} = \boldsymbol{0} \text{ on } \Gamma_D \; .$$

Along the Neumann boundary Γ_N the structure is free of stress and we impose

$$\boldsymbol{\sigma}\boldsymbol{\nu}_S = \boldsymbol{0} \text{ on } \Gamma_N \; .$$

The strain tensor is the symmetric part of grad $\boldsymbol{u}$ and can therefore be rewritten in terms of grad $\boldsymbol{u}$ and its skew-symmetric part, based on the formulations in [5],

$$\begin{aligned} \epsilon(\boldsymbol{u}) &= \text{grad } \boldsymbol{u} - sk(\text{grad } \boldsymbol{u}) \\ &= \text{grad } \boldsymbol{u} - (-1)^d m\boldsymbol{\chi} \; . \end{aligned}$$

The skew-symmetric matrix $\boldsymbol{\chi}$ is defined in Section 2.1. The newly introduced variable m is a scalar in the two-dimensional setting and a vector for the three-dimensional setting, in which case the last product is substituted by the dot-product. The variable represents the vorticity, defined by $m = \frac{1}{2}\nabla \times \boldsymbol{u}$. In two dimensions, this yields $m = \frac{\partial u_y}{\partial_x} - \frac{\partial u_x}{\partial_y}$. Note that when substituting the strain tensor in the constitutive equation, symmetry of the stress tensor is no longer implied. Hence, we impose the following symmetry condition:

$$sk(\boldsymbol{\sigma}) = \boldsymbol{0} \text{ in } \Omega_S \; .$$

The governing equations of the solid domain can be summarized by

$$\begin{aligned} &\text{div } \boldsymbol{\sigma} + \boldsymbol{f}_S = \boldsymbol{0} && \text{in } \Omega_S \; , \\ &\mathcal{C}^{-1}\boldsymbol{\sigma} - \text{grad } \boldsymbol{u} + (-1)^d m\boldsymbol{\chi} = \boldsymbol{0} && \text{in } \Omega_S \; , \\ &sk(\boldsymbol{\sigma}) = \boldsymbol{0} && \text{in } \Omega_S \; , \\ &\boldsymbol{u} = 0 && \text{on } \Gamma_D \; , \\ &\boldsymbol{\sigma}\boldsymbol{\nu}_S = \boldsymbol{0} && \text{on } \Gamma_N \; , \end{aligned}$$

together with coupling conditions along the interface Σ, which are still to be determined.

For the fluid domain the quantity of interest is pressure. The sound propagation in fluid is described by the wave equation, which simplifies to the Helmholz equation for time harmonic sound pressure. The governing equation then reads

$$\text{div grad } p = -\frac{\omega^2}{c^2} p \quad \text{in } \Omega_F \quad ,$$

where c describes the velocity of the sound pressure wave, also known as the acoustic speed, and is assumed to be constant. The frequencies are denoted by ω. We capture the right-hand side by the source term $f_F = \frac{\omega^2}{c^2} p$. The fluid domain is entirely surrounded by the solid domain. Hence, no boundary conditions except for the interface conditions are given. Since a least-squares finite element approach requires a first order system, we introduce the pressure gradient $\boldsymbol{\pi}$. The constitutive equation for the fluid domain then reads

$$\boldsymbol{\pi} - \text{grad } p = \mathbf{0} \quad \text{in } \Omega_F \ ,$$

and the governing equations rewrites to

$$\text{div } \boldsymbol{\pi} = -f_F \quad \text{in } \Omega_F \ .$$

We can hence summarize the governing equations for the fluid domain as

$$\begin{aligned} \boldsymbol{\pi} - \text{grad } p &= \mathbf{0} \quad \text{in } \Omega_F \ , \\ \text{div } \boldsymbol{\pi} + f_F &= 0 \quad \text{in } \Omega_F \ . \end{aligned}$$

It remains to specify the coupling conditions along the interface Σ. Here, we have a kinetic condition coupling the stress on the interface to the pressure exerted on the fluid (action-reaction principle) and a kinematic condition, describing the fluid and solid in contact without friction at the interface (slip condition), as is more thoroughly described in [1]. The two principles lead to coupling conditions of the form

$$\begin{aligned} \boldsymbol{\sigma \nu_F} + p \boldsymbol{\nu}_F &= \mathbf{0} \quad && \text{on } \Sigma \ , \\ \frac{\partial p}{\partial \boldsymbol{\nu}_F} + \frac{\rho_F}{\rho_S} \text{div } \boldsymbol{\sigma} \cdot \boldsymbol{\nu}_F &= \mathbf{0} \quad && \text{on } \Sigma \ , \end{aligned}$$

where we introduce the solid and fluid densities ρ_S and ρ_F, respectively. Substituting the pressure gradient and the solid source term, the second equation simplifies to

$$\boldsymbol{\pi} \cdot \boldsymbol{\nu}_F - \frac{\rho_F}{\rho_S} \boldsymbol{f}_S \cdot \boldsymbol{\nu}_F = \mathbf{0} \quad \text{on } \Sigma \ .$$

The model for the coupled system then reads

$$\begin{aligned}
&\operatorname{div} \boldsymbol{\sigma} + \boldsymbol{f}_S = \mathbf{0} && \text{in } \Omega_S \ , \\
&\mathcal{C}^{-1}\boldsymbol{\sigma} - \operatorname{grad} \boldsymbol{u} + (-1)^d m \boldsymbol{\chi} = \mathbf{0} && \text{in } \Omega_S \ , \\
&sk(\boldsymbol{\sigma}) = \mathbf{0} && \text{in } \Omega_S \ , \\
&\boldsymbol{\pi} - \operatorname{grad} p = \mathbf{0} && \text{in } \Omega_F \ , \\
&\operatorname{div} \boldsymbol{\pi} + f_F = 0 && \text{in } \Omega_F \ , \\
&\boldsymbol{u} = 0 && \text{on } \Gamma_D \ , \\
&\boldsymbol{\sigma}\boldsymbol{\nu}_S = \mathbf{0} && \text{on } \Gamma_N \ , \\
&\boldsymbol{\sigma}\boldsymbol{\nu}_F + p\boldsymbol{\nu}_F = 0 && \text{on } \Sigma \ , \\
&\boldsymbol{\pi} \cdot \boldsymbol{\nu}_F - \frac{\rho_F}{\rho_S} \boldsymbol{f}_S \cdot \boldsymbol{\nu}_F = 0 && \text{on } \Sigma \ .
\end{aligned}$$

When formulating the eigenproblem the source terms are replaced by the eigenfunctions $\boldsymbol{f}_S = \omega^2 \rho_S \boldsymbol{u}$ and $f_F = \frac{\omega^2}{c^2} p$ with $\omega \in \mathbb{R}$ the corresponding eigenvalue.

In the solid domain the unknowns $\boldsymbol{\sigma}$, $\boldsymbol{u}$ and m are naturally sought in $\boldsymbol{H}(div; \Omega_S)$, $\boldsymbol{H}^1(\Omega_S)$ and $L^2(\Omega_S)$, respectively. In the fluid domain the pressure p is naturally found in $H^1(\Omega_F)$ whereas the pressure gradient $\boldsymbol{\pi}$ is naturally found in $H(div; \Omega_F)$. With these natural solution spaces the trace spaces on the interface do not coincide (see [10, Chapter III.1]). Traces of $H(div)$ functions are, in general, not in $L^2(\partial\Omega)$. Indeed, we observe $\boldsymbol{\sigma}\boldsymbol{\nu}_F \in \boldsymbol{H}^{-1/2}(\Sigma)$ whereas $p\boldsymbol{\nu}_F \in \boldsymbol{H}^{1/2}(\Sigma) \subset \boldsymbol{L}^2(\Sigma)$ and similarly, $\boldsymbol{\pi} \cdot \boldsymbol{\nu}_F \in H^{-1/2}(\Sigma)$ and $\boldsymbol{f}_S \cdot \boldsymbol{\nu}_F \in H^{-1/2}(\Sigma)$ for $\boldsymbol{f}_S \in \boldsymbol{L}^2(\Omega_S)$. For the source term we can assume sufficient regularity, i. e. $\boldsymbol{f}_S \in \boldsymbol{H}^1(\Omega)$, to ensure $\boldsymbol{f}_S \cdot \boldsymbol{\nu}_F \in H^{1/2}(\Sigma) \subset L^2(\Sigma)$. In fact, this will be the case in the eigenvalueproblem when $\boldsymbol{f}_S = \frac{\omega^2}{\rho_S} \boldsymbol{u}$. The solution spaces for the stress and pressure gradient are restricted to $\bar{\boldsymbol{H}}(div; \Omega_S)$ and $\bar{H}(div; \Omega_F)$ defined in Section 2.1. It follows that the interface conditions are now defined on $\boldsymbol{L}^2(\Sigma)$ and $L^2(\Sigma)$, respectively. The Dirichlet and Neumann boundary conditions of the solid domain can easily be incorporated into the function spaces. We therefore search for the displacement $\boldsymbol{u} \in \boldsymbol{H}^1_{\Gamma_D}(\Omega_S)$ and the stress tensor $\boldsymbol{\sigma} \in \bar{\boldsymbol{H}}_{\Gamma_N}(div; \Omega_S)$. We conclude by defining the product function space

$$\mathcal{W} \coloneqq \bar{\boldsymbol{H}}_{\Gamma_N}(div; \Omega_S) \times \boldsymbol{H}^1_{\Gamma_D}(\Omega_S) \times L^2(\Omega_S) \times \bar{H}(div; \Omega_F) \times H^1(\Omega_F) \tag{9}$$

with the associated norm

$$\begin{aligned}
\|(\boldsymbol{\tau}, \boldsymbol{v}, n, \boldsymbol{\xi}, q)\|^2_{\mathcal{W}} = \|\boldsymbol{\tau}\|^2_{H(div;\Omega_S)} + \|\boldsymbol{\tau}\boldsymbol{\nu}_S\|^2_{L^2(\Sigma)} + \|\boldsymbol{v}\|^2_{H^1(\Omega_S)} + \|n\|^2_{L^2(\Omega_S)} \\
+ \|\boldsymbol{\xi}\|^2_{H(div;\Omega_F)} + \|\boldsymbol{\xi} \cdot \boldsymbol{\nu}_F\|^2_{L^2(\Sigma)} + \|q\|^2_{H^1(\Omega_F)} \ .
\end{aligned} \tag{10}$$

To shorten notation, we replace the subscripts in the notation of the L^2 inner products and norms. The norms will be denoted by

$$\|\cdot\|_{L^2(\Omega_S)} = \|\cdot\|_S \ , \|\cdot\|_{L^2(\Omega_F)} = \|\cdot\|_F \ \text{ and } \ \|\cdot\|_{L^2(\Sigma)} = \|\cdot\|_\Sigma \ ,$$

the inner products by

$$\langle\cdot,\cdot\rangle_{L^2(\Omega_S)} = \langle\cdot,\cdot\rangle_S \ , \langle\cdot,\cdot\rangle_{L^2(\Omega_F)} = \langle\cdot,\cdot\rangle_F \ , \ \text{ and } \ \langle\cdot,\cdot\rangle_{L^2(\Sigma)} = \langle\cdot,\cdot\rangle_\Sigma \ .$$

All remaining norms and inner products are indicated in the usual way.

The fluid-structure interaction problem then reads: For given $\boldsymbol{f}_S \in \boldsymbol{H}^1(\Omega_S)$ and $f_F \in L^2(\Omega_F)$ find $(\boldsymbol{\sigma}, \boldsymbol{u}, m, \boldsymbol{\pi}, p) \in \mathcal{W}$ such that

$$
\begin{aligned}
&\operatorname{div} \boldsymbol{\sigma} + \boldsymbol{f}_S = \boldsymbol{0} && \text{in } \Omega_S \ , \\
&\mathcal{C}^{-1}\boldsymbol{\sigma} - \operatorname{grad} \boldsymbol{u} + (-1)^d m \boldsymbol{\chi} = \boldsymbol{0} && \text{in } \Omega_S \ , \\
&sk(\boldsymbol{\sigma}) = \boldsymbol{0} && \text{in } \Omega_S \ , \\
&\boldsymbol{\pi} - \operatorname{grad} p = \boldsymbol{0} && \text{in } \Omega_F \ , \\
&\operatorname{div} \boldsymbol{\pi} + f_F = 0 && \text{in } \Omega_F \ , \\
&\boldsymbol{\sigma}\boldsymbol{\nu}_F + p\boldsymbol{\nu}_F = 0 && \text{on } \Sigma \ , \\
&\boldsymbol{\pi} \cdot \boldsymbol{\nu}_F - \frac{\rho_F}{\rho_S} \boldsymbol{f}_S \cdot \boldsymbol{\nu}_F = 0 && \text{on } \Sigma \ .
\end{aligned}
\tag{11}
$$

3 Finite Element Spaces

In this section we introduce the finite element spaces that will be used in the analysis and computation of the LSFEM formulation of the fluid-structure interaction. For each space, we provide the basis functions and corresponding interpolation error bounds. We assume $\mathcal{T}_h$ to be a regular, triangular partition of the domain Ω. Furthermore, h denotes the mesh size which we assume to be constant for all elements. We will denote edges by $(e_i)_i$ and vertices by $(x_i, y_i)_i$.

3.1 Finite Element Approximation of $H^1(\Omega)$

The standard conforming finite element space for functions in $H^1(\Omega)$ is the space of continuous piecewise polynomial functions, see for example [13, Chapter 1.1]. For a given partition $\mathcal{T}$ of the domain Ω we define $\mathcal{V}_h^k \subset H^1(\Omega)$ as

$$\mathcal{V}_h^k \coloneqq \{\phi \in \mathcal{C}(\Omega) : \phi|_T \in \mathcal{P}_k(T),\ \forall\ T \in \mathcal{T}_h\}\ .$$

Here, we introduced

- $P_k(T)$: The space of polynomials of degree $\leq k$ on an element T,
- $C(\Omega)$: The space of continuous functions over Ω.

The finite dimensional space can be spanned by a set of basis functions, ϕ_i, $\ 1 \leq i \leq N_h$. Lagrangian basis functions are the common choice. The polynomials in two dimensions are formed by

$$L_{ij}(\boldsymbol{x}) = L_i(x)L_j(y)$$

with the Lagrange polynomial

$$L_i(x) = \prod_{s=0, s\neq i}^{k} \frac{(x - x_s)}{(x_i - x_s)}\ ,$$

for given degrees of freedom (*d.o.f.*), (x_s, y_s). Lagrangian basis functions barely overlap, resulting in sparse linear systems, which in turn allow for efficient computations. Furthermore, interelement continuity is preserved when choosing the degrees of freedom appropriately. The standard choice of d.o.f. are depicted in Figure 2 and Figure 3 for first and second order approximations. For higher order functions interior d.o.f. are included. The local interpolation operator $\rho_h : H^1(T) \to P_k(T)$ is then constructed to map functions v to its finite element approximation $\rho_h(v)$. Note that $\rho_h(p_k) = p_k$ for all $p_k \in P_k(T)$.
To make a meaningful approximation estimate for piecewise polynomial elements we need to restrict the solution space to admit smoothness at least implied by $H^2(\Omega)$. More precisely, we can state the following interpolation estimate, [10, Chapter III.2, Proposition 2.2.2]:

Theorem 3.1 (Approximation Properties Piecewise Polynomial Elements)**.** *Let $(\mathcal{T}_h)_{h\geq 0}$ be a regular family of affine partitions and let $\rho_h : H^1(T) \to P_k(T)$ describe the local interpolation operator for all $T \in (\mathcal{T}_h)$ as above. Assume $v \in H^s(\Omega)$ with $1 \leq s \leq k+1$. Then there exists a constant c independent of h such that*

$$\|\rho_h(v) - v\|_{L^2(T)} \leq ch^s|v|_{H^s(\Delta T)}$$
$$\|grad(\rho_h(v) - v)\|_L^2(T) \leq ch^{s-1}|v|_{H^s(\Delta T)}$$

where

$$\Delta T := \{T' \mid \bar{T}' \cap \bar{T} \neq \emptyset\}$$

the set of all neighbouring elements.

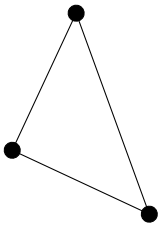

Figure 2: D.o.f. of the first order Lagrangian element

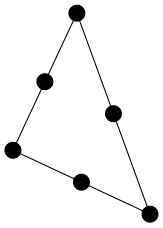

Figure 3: D.o.f. of the second order Lagrangian element.

3.2 Finite Element Approximation of $L^2(\Omega)$

The standard conforming finite elements space for $L^2(\Omega)$ are piecewise polynomials of order k,

$$\mathcal{V}_h^k := \{\phi \in L^2(\Omega) : \phi|_T \in P_k(T),\ \forall T \in \mathcal{T}_h\}\ .$$

A zeroth order approximation leads to a piecewise constant function as the finite element approximation, a first order approximation results in piecewise linear functions being used. Since we do not require continuity of the elements in this setting the d.o.f. are allowed to lie within the element. The d.o.f. are depicted in Figures 4 and 5. We denote the interpolation of v by $\rho_h(v)$, as in the previous section. To make any meaningful approximations properties we need to restrict the solution space to $H^1(\Omega)$. We then can formulate an approximation error bound in a similar fashion as before, ([10, Chapter III.2, Proposition 2.2.2]):

Theorem 3.2 (Approximation Properties of Polynomial Elements)**.** *If $(\mathcal{T}_h)_{h\geq 0}$ is a regular family of affine partitions and $\rho_h : L^2(T) \to P_k(T)$ the local interpolation operator for all $T \in (\mathcal{T}_h)$ described above. Assume $v \in H^s(\Omega)$ with $1 \leq s \leq k+1$. Then there exists a constant c independent of h such that*

$$\|\rho_h(v) - v\|_{L^2(T)} \leq ch^s |v|_{H^s(T)}\ .$$

3.3 Finite Element Approximation of $H(div;\Omega)$

A suitable finite element space for $H(div)$-spaces can be formed using Raviart-Thomas elements. Raviart-Thomas elements (*RT-elements*) are vector-valued elements and are very well suited to approximate the space $H(div;\Omega)$, see [10, Chapter III.3]. The definitions of RT-elements differ slightly across literature, in particular the definition of the order of the elements varies. In what follows, we will use the notation presented in [10, Chapter 3] and [13, Chapter 1], though we already note a change in definition when presenting the

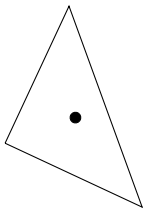

Figure 4: D.o.f. for zeroth order discontinuous elements.

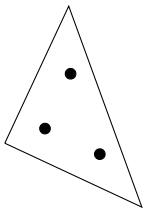

Figure 5: D.o.f. for first order discontinuous elements.

implementations in Chapter 5.2. On a triangular element T RT-elements of order k are defined by

$$RT_k(T) = (P_k(T))^2 + \boldsymbol{x}P_k(T) \ ,$$

with $P_k(T)$ the polynomial space defined earlier and $(P_k(T))^2$ the space of vector-valued polynomials. The finite element space is then constructed as

$$\mathcal{V}_h^k \coloneqq \{\boldsymbol{\phi} \in H(div;\Omega) \ : \ \boldsymbol{\phi}|_T \in RT_k(T), \ \forall T \in \mathcal{T}_h\} \ .$$

The basis functions are described by $dim(RT_k(T)) = (k+1)(k+3)$ degrees of freedom. The d.o.f. for the lowest order Raviart-Thomas element lie on the edges of the cell and describe the value of the normal component of the flux across the faces. For higher order RT-elements interior d.o.f. are added, see Figure 6 and Figure 7. The local interpolation operator $\rho_h : \bar{H}(div;T) \to RT_k(T)$ is defined by

$$\begin{aligned}
&\int_{\partial T} (\boldsymbol{\phi} - \rho_h\boldsymbol{\phi}) \cdot \boldsymbol{\nu} \ p_k \ d\Gamma = 0, \ \forall \ p_k \in R_k(\partial T) \ \text{ for } k \geq 0, \\
&\int_T (\boldsymbol{\phi} - \rho_h\boldsymbol{\phi}) \cdot \boldsymbol{p}_{k-1} \ d\Omega = 0, \ \forall \ \boldsymbol{p}_{k-1} \in (P_{k-1}(T))^2 \ \text{ for } k \geq 1 \ .
\end{aligned}$$

Note that we have used a more restricted space $\bar{H}(div;T)$ to ensure $\boldsymbol{\phi}\cdot\boldsymbol{\nu} \in H^{1/2}(\partial T)$. We furthermore introduced the space

- $R_k(\partial T)$: The space of polynomials of degree $\leq k$ on each side of T,

  $$R_k(\partial T) = \{\phi \mid \phi \in L^2(\partial T), \ \phi|_{e_i} \in P_k(e_i), \ \forall e_i\}$$

  where e_i, $1 \leq i \leq 3$, denote the edges of T.

One reason RT-elements approximate the $H(div)$-space well is that its divergence maps onto the space of piecewise polynomial functions, see for example [10, Proposition 3.2]:

Theorem 3.3 (Divergence of RT-elements)**.** *For a triangular element T we have for $\boldsymbol{\phi} \in RT_k(T)$*

$$div \ \boldsymbol{\phi} \in P_k(T) \quad \text{and} \quad \boldsymbol{\phi}\cdot\boldsymbol{\nu}|_{\partial T} \in R_k(\partial T) \ .$$

This ensures a good approximation of the divergence in $L^2(\Omega)$ and continuity of the normal component along edges. Note that tangential components along an edge may be discontinuous. For the lowest-order elements on a regular triangular mesh the local shape function for the ith edge is given by

$$\boldsymbol{\theta}_i(\boldsymbol{x}) = \frac{1}{2|T|}(\boldsymbol{x} - \boldsymbol{x}_i)$$

with $\boldsymbol{x}_i$ denoting the opposite vertex. We can state the following approximation property, see [10, Chapter III.3; Proposition 3.9]

Theorem 3.4 (Approximation Properties Raviart-Thomas Elements)**.** *Let $\mathcal{T}_h$ be a regular family of affine partitions, and let ρ_h: $\bar{H}(div;T) \to RT_k(T)$ be defined as above for every $T \in \mathcal{T}_h$. Furthermore, assume $\boldsymbol{\xi} \in \boldsymbol{H}^s(T) \cap H(div;T)$ and $div\, \boldsymbol{\xi} \in H^s(T)$ for $0 \leq s \leq k+1$. Then there exists a constant c independent of h such that*

$$\|\boldsymbol{\xi} - \rho_h(\boldsymbol{\xi})\|_{L^2(T)} \leq ch^s |\boldsymbol{\xi}|_{H^s(T)} \ .$$

Moreover,

$$\|div(\boldsymbol{\xi} - \rho_h(\boldsymbol{\xi}))\|_{L^2(T)} \leq ch^s |div\, \boldsymbol{\xi}|_{H^s(T)} \ .$$

When applying the approximation property one has to pay attention to two things. Firstly, similar to the piecewise polynomial case, stronger regularity needs to be imposed on the solution space in order to obtain a converging approximation property. More precisely, one would require $\boldsymbol{\xi} \in \bar{H}(div;T) \cap \boldsymbol{H}^1(T)$ and div $\boldsymbol{\xi} \in H^1(T)$. Secondly, for a function $\boldsymbol{\xi}$ to be in $\bar{H}(div;T)$ it is not sufficient to assume $\boldsymbol{\xi} \in \bar{H}(div;\Omega)$. To ensure $\boldsymbol{\xi} \in \bar{H}(div;T)$ one can restrict the solution space to $H(div;\Omega) \cap \boldsymbol{L}^s(\Omega)$, $s > 2$, like is done in [10, Chapter III.3.4] or ensure, as before $\boldsymbol{\xi} \in \bar{H}(div;\Omega) \cap \boldsymbol{H}^1(\Omega)$.

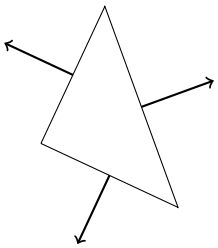

Figure 6: D.o.f. of the zeroth order Raviart-Thomas Element.

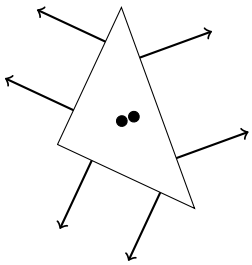

Figure 7: D.o.f. of the first order Raviart-Thomas Element.

4 Least-Squares Functional and Finite Element Approximation

In this section we formulate the least-squares functional and define the corresponding minimization problem. Subsequently, the weak formulation is derived. As already mentioned in the first section of this thesis, the least-squares functional can be formulated in various ways. One choice presents itself in the way in which boundary and interface conditions are imposed. This can be done strongly, by imposing them on the solution space, or weakly, by adding auxiliary terms to the least-squares functional. We will develop both formulations, with strong and weak boundary conditions, respectively, in the next two sections. However, we will only continue analysing the latter in terms of existence, uniqueness and error estimates in the last sections of this chapter. These results for the formulation with strongly imposed boundary conditions can be derived in a similar way.

4.1 Formulation with Strong Interface Conditions

For the formulation with strong boundary and interface conditions all conditions are imposed on the solution space. In the problem of equation (11) this relates to the last two equation defined for Σ, as well as the Dirichlet and Neumann boundary conditions. We hence define the space, for given $\boldsymbol{f}_S \in \boldsymbol{H}^1(\Omega_S)$

$$\hat{\mathcal{W}} \coloneqq \{(\boldsymbol{\tau}, \boldsymbol{v}, n, \boldsymbol{\xi}, q) \in \mathcal{W} \mid \boldsymbol{\tau}\boldsymbol{\nu}_F = -q\boldsymbol{\nu}_F \text{ and } \boldsymbol{\xi} \cdot \boldsymbol{\nu}_F = \frac{\rho_F}{\rho_S} \boldsymbol{f}_S \cdot \boldsymbol{\nu}_F \text{ on } \Sigma\}$$

with the space $\mathcal{W}$ defined in (9). For a given $\boldsymbol{f}_S \in \boldsymbol{H}^1(\Omega_S)$ and $f_F \in L^2(\Omega_F)$ the simplest least-squares functional for problem (11) is given below. We denote this functional by $\hat{F} : \hat{\mathcal{W}} \to \mathbb{R}$, which is defined as

$$\begin{aligned}\hat{F}(\boldsymbol{\tau}, \boldsymbol{v}, n, \boldsymbol{\xi}, q; \boldsymbol{f}_S, f_F) = \|\text{div } \boldsymbol{\tau} + \boldsymbol{f}_S\|_S^2 + \|\mathcal{C}^{-1}\boldsymbol{\tau} - \text{grad } \boldsymbol{v} + n\boldsymbol{\chi}\|_S^2 + \|sk(\boldsymbol{\tau})\|_S^2 \\ + \|\boldsymbol{\xi} - \text{grad } q\|_F^2 + \|\text{div } \boldsymbol{\xi} + f_F\|_F^2 \quad ,\end{aligned}$$

where we considered the L^2-norms on the fluid and structure domain. The least-squares method seeks the minimizer $(\boldsymbol{\sigma}, \boldsymbol{u}, m, \boldsymbol{\pi}, p) \in \hat{\mathcal{W}}$ of $\hat{F}$,

$$\arg \min_{(\boldsymbol{\tau}, \boldsymbol{v}, n, \boldsymbol{\xi}, q) \in \hat{\mathcal{W}}} \hat{F}(\boldsymbol{\tau}, \boldsymbol{v}, n, \boldsymbol{\xi}, q; \boldsymbol{f}_S, f_F) \ .$$

The variational formulation is obtained by applying the first order necessary condition on each variable,

$$\begin{aligned}\frac{\partial}{\partial\theta} \hat{F}(\boldsymbol{\tau} + \theta\boldsymbol{\sigma}, \boldsymbol{v}, n, \boldsymbol{\xi}, q) \mid_{\theta=0} = 0 \ , \\ \frac{\partial}{\partial\theta} \hat{F}(\boldsymbol{\tau}, \boldsymbol{v} + \theta\boldsymbol{u}, n, \boldsymbol{\xi}, q) \mid_{\theta=0} = 0 \ , \\ \frac{\partial}{\partial\theta} \hat{F}(\boldsymbol{\tau}, \boldsymbol{v}, n + \theta m, \boldsymbol{\xi}, q) \mid_{\theta=0} = 0 \ , \\ \frac{\partial}{\partial\theta} \hat{F}(\boldsymbol{\tau}, \boldsymbol{v}, n, \boldsymbol{\xi} + \theta\boldsymbol{\pi}, q) \mid_{\theta=0} = 0 \ .\end{aligned}$$

This yields the variational formulation: Find $(\boldsymbol{\sigma}, \boldsymbol{u}, m, \boldsymbol{\pi}, p) \in \hat{\mathcal{W}}$ such that

$$\begin{aligned}
&\langle \operatorname{div} \boldsymbol{\sigma}, \operatorname{div} \boldsymbol{\tau}\rangle_S + \langle \mathcal{C}^{-1}\boldsymbol{\sigma}, \mathcal{C}^{-1}\boldsymbol{\tau}\rangle_S + \langle sk(\boldsymbol{\sigma}), sk(\boldsymbol{\tau})\rangle_S \\
&\quad - \langle \operatorname{grad} \boldsymbol{u}, \mathcal{C}^{-1}\boldsymbol{\tau}\rangle_S - \langle \mathcal{C}^{-1}\boldsymbol{\sigma}, \operatorname{grad} \boldsymbol{v}\rangle_S \\
&\quad + \langle \operatorname{grad} \boldsymbol{u}, \operatorname{grad} \boldsymbol{v}\rangle_S \\
&\quad - \langle \operatorname{curl} \boldsymbol{u}, n\rangle_S - \langle \operatorname{curl} \boldsymbol{v}, m\rangle_S \\
&\quad + \langle m\boldsymbol{\chi}, \mathcal{C}^{-1}\boldsymbol{\tau}\rangle_S + \langle \mathcal{C}^{-1}\boldsymbol{\sigma}, n\boldsymbol{\chi}\rangle_S \\
&\quad + 2mn \\
&\quad + \langle \boldsymbol{\pi}, \boldsymbol{\xi}\rangle_F + \langle \operatorname{div} \boldsymbol{\pi}, \operatorname{div} \boldsymbol{\xi}\rangle_F \\
&\quad - \langle \operatorname{grad} p, \boldsymbol{\xi}\rangle_F - \langle \boldsymbol{\pi}, \operatorname{grad} q\rangle_F \\
&\quad + \langle \operatorname{grad} p, \operatorname{grad} q\rangle_F \\
&= -\langle \boldsymbol{f}_S, \operatorname{div} \boldsymbol{\tau}\rangle_S - \langle f_F, \operatorname{div} \boldsymbol{\xi}\rangle_F \ .
\end{aligned}$$

The related eigenvalue problem is obtained by setting $\boldsymbol{f_S} = \omega^2 \rho_S \boldsymbol{u}$, $f_F = \frac{\omega^2}{c^2} p$.

One reason for not further exploring this approach is the difficulty in which the finite element space would need to be constructed, which would lead to complicated numerical implementations. However, properties of the continuous formulations follow in the same way as for the weakly imposed formulation, as described in the remainder of this section.

4.2 Formulation with Weak Interface Conditions

Imposing the interface conditions weakly requires additional terms in the least-squares functional. The straightforward way to do this is by measuring the residual of the interface terms in the fractional Sobolev norm. Here, we need the additional requirements $\boldsymbol{\tau}\boldsymbol{\nu}_F \in \boldsymbol{H}^{1/2}(\Sigma)$ and $\boldsymbol{\xi} \cdot \boldsymbol{\nu}_F \in H^{1/2}(\Sigma)$. The solution space is then denoted by $\tilde{\mathcal{W}}$, defined by $\mathcal{W}$ of equation (9) with these additional constraints. The associated norm reads

$$\begin{aligned}
\|(\boldsymbol{\tau}, \boldsymbol{v}, n, \boldsymbol{\xi}, q)\|^2_{\tilde{\mathcal{W}}} = \|\boldsymbol{\tau}\|^2_{H(div;\Omega_S)} + \|\boldsymbol{\tau}\boldsymbol{\nu}_S\|^2_{H^{1/2}(\Sigma)} + \|\boldsymbol{v}\|^2_{H^1(\Omega_S)} + \|n\|^2_{L^2(\Omega_S)} \\
+ \|\boldsymbol{\xi}\|^2_{H(div;\Omega_F)} + \|\boldsymbol{\xi} \cdot \boldsymbol{\nu}_F\|^2_{H^{1/2}(\Sigma)} + \|q\|^2_{H^1(\Omega_F)} \ .
\end{aligned}$$

For given $\boldsymbol{f}_S \in \boldsymbol{H}^1(\Omega_S)$ and $f_F \in L^2(\Omega_F)$ this yields the functional, $\tilde{F} : \tilde{\mathcal{W}} \to \mathbb{R}$,

$$\begin{aligned}
\tilde{F}(\boldsymbol{\tau}, \boldsymbol{v}, n, \boldsymbol{\xi}, q; \boldsymbol{f}_S, f_F) = \|\operatorname{div} \boldsymbol{\tau} + \boldsymbol{f}_S\|^2_S + \|\mathcal{C}^{-1}\boldsymbol{\tau} - \operatorname{grad} \boldsymbol{v} + n\boldsymbol{\chi}\|^2_S + \|sk(\boldsymbol{\tau})\|^2_S \\
+ \|\boldsymbol{\xi} - \operatorname{grad} q\|^2_F + \|\operatorname{div} \boldsymbol{\xi} + f_F\|^2_F \\
+ \|\boldsymbol{\tau}\boldsymbol{\nu}_F + q\boldsymbol{\nu}_F\|^2_{H^{1/2}(\Sigma)} + \|\boldsymbol{\xi} \cdot \boldsymbol{\nu}_F - \frac{\rho_F}{\rho_S} \boldsymbol{f}_S \cdot \boldsymbol{\nu}_F\|^2_{H^{1/2}(\Sigma)} \ ,
\end{aligned}$$

However, the fractional Sobolev norm requires the evaluation of $H^{1/2}$ norms and inner products, resulting in an impractical least-squares method. The simplest way to circumvent these difficulties is to replace the $H^{1/2}(\partial\Omega)$-norm by the $L^2(\partial\Omega)$-norm. However, this procedure results in suboptimal results, prone the loss of accuracy, as demonstrated in [15, Chapter 12]. Stevenson elaborates on this problem in [23]. Despite this disadvantage we have decided to pursue this approach, due to its simplicity and practicality. The

least-squares functional is adjusted to

$$\begin{aligned} F(\boldsymbol{\tau},\boldsymbol{v},n,\boldsymbol{\xi},q;\boldsymbol{f}_S,f_F) = {} & \|\mathrm{div}\ \boldsymbol{\tau}+\boldsymbol{f}_S\|_S^2 + \|\mathcal{C}^{-1}\boldsymbol{\tau}-\mathrm{grad}\ \boldsymbol{v}+n\boldsymbol{\chi}\|_S^2 + \|sk(\boldsymbol{\tau})\|_S^2 \\ & + \|\boldsymbol{\xi}-\mathrm{grad}\ q\|_F^2 + \|\mathrm{div}\ \boldsymbol{\xi}+f_F\|_F^2 \\ & + \|\boldsymbol{\tau}\boldsymbol{\nu}_F+q\boldsymbol{\nu}_F\|_\Sigma^2 + \|\boldsymbol{\xi}\cdot\boldsymbol{\nu}_F-\frac{\rho_F}{\rho_S}\boldsymbol{f}_S\cdot\boldsymbol{\nu}_F\|_\Sigma^2\ . \end{aligned} \tag{12}$$

The least-squares method seeks the minimizer $(\boldsymbol{\sigma},\boldsymbol{u},m,\boldsymbol{\pi},p)\in\mathcal{W}$ of F,

$$\arg\min_{(\boldsymbol{\tau},\boldsymbol{v},n,\boldsymbol{\xi},q)\in\mathcal{W}} F(\boldsymbol{\tau},\boldsymbol{v},n,\boldsymbol{\xi},q;\boldsymbol{f}_S,f_F)\ .$$

Applying the first order condition yields the variational formulation: Find $(\boldsymbol{\sigma},\boldsymbol{u},m,\boldsymbol{\pi},p)\in\mathcal{W}$ such that

$$\begin{aligned} & \langle\mathrm{div}\ \boldsymbol{\sigma},\mathrm{div}\ \boldsymbol{\tau}\rangle_S + \langle\mathcal{C}^{-1}\boldsymbol{\sigma},\mathcal{C}^{-1}\boldsymbol{\tau}\rangle_S + \langle sk(\boldsymbol{\sigma}),sk(\boldsymbol{\tau})\rangle_S \\ & \quad - \langle\mathrm{grad}\ \boldsymbol{u},\mathcal{C}^{-1}\boldsymbol{\tau}\rangle_S - \langle\mathcal{C}^{-1}\boldsymbol{\sigma},\mathrm{grad}\ \boldsymbol{v}\rangle_S \\ & \quad + \langle\mathrm{grad}\ \boldsymbol{u},\mathrm{grad}\ \boldsymbol{v}\rangle_S \\ & \quad - \langle\mathrm{curl}\ \boldsymbol{u},n\rangle_S - \langle\mathrm{curl}\ \boldsymbol{v},m\rangle_S \\ & \quad + \langle m\boldsymbol{\chi},\mathcal{C}^{-1}\boldsymbol{\tau}\rangle_S + \langle\mathcal{C}^{-1}\boldsymbol{\sigma},n\boldsymbol{\chi}\rangle_S \\ & \quad + 2mn \\ & \quad + \langle\boldsymbol{\pi},\boldsymbol{\xi}\rangle_F + \langle\mathrm{div}\ \boldsymbol{\pi},\mathrm{div}\ \boldsymbol{\xi}\rangle_F \\ & \quad - \langle\mathrm{grad}\ p,\boldsymbol{\xi}\rangle_F + \langle\boldsymbol{\pi},\mathrm{grad}\ q\rangle_F \\ & \quad + \langle\mathrm{grad}\ p,\mathrm{grad}\ q\rangle_F \\ & \quad + \langle\boldsymbol{\sigma}\boldsymbol{\nu}_F,\boldsymbol{\tau}\boldsymbol{\nu}_F\rangle_\Sigma \\ & \quad + \langle p\boldsymbol{\nu}_F,\boldsymbol{\tau}\boldsymbol{\nu}_F\rangle_\Sigma + \langle\boldsymbol{\sigma}\boldsymbol{\nu}_F,q\boldsymbol{\nu}_F\rangle_\Sigma \\ & \quad + \langle\boldsymbol{\pi}\cdot\boldsymbol{\nu}_F,\boldsymbol{\xi}\cdot\boldsymbol{\nu}_F\rangle_\Sigma + \langle p\boldsymbol{\nu}_F,q\boldsymbol{\nu}_F\rangle_\Sigma \\ & = -\langle\boldsymbol{f}_S,\mathrm{div}\ \boldsymbol{\tau}\rangle_S - \langle f_F,\mathrm{div}\ \boldsymbol{\xi}\rangle_F + \langle\frac{\rho_F}{\rho_S}\boldsymbol{f}_S\cdot\boldsymbol{\nu}_F,\boldsymbol{\xi}\cdot\boldsymbol{\nu}_F\rangle_\Sigma\ . \end{aligned} \tag{13}$$

By verifying that each term on the left-hand side is symmetric, the symmetry of the entire left-hand side may be observed. Substituting the eigenvalues and eigenfunctions for the source terms, $\boldsymbol{f_S}=\omega^2\rho_S\boldsymbol{u}$, $f_F=\frac{\omega^2}{c^2}p$, yields the eigenproblem:

Find $\omega \in \mathbb{R}$, $(\boldsymbol{\sigma}, \boldsymbol{u}, m, \boldsymbol{\pi}, p) \in \mathcal{W}$ such that

$$
\begin{aligned}
&\langle \text{div } \boldsymbol{\sigma}, \text{div } \boldsymbol{\tau} \rangle_S + \langle \mathcal{C}^{-1}\boldsymbol{\sigma}, \mathcal{C}^{-1}\boldsymbol{\tau} \rangle_S + \langle sk(\boldsymbol{\sigma}), sk(\boldsymbol{\tau}) \rangle_S \\
&\quad - \langle \text{grad } \boldsymbol{u}, \mathcal{C}^{-1}\boldsymbol{\tau} \rangle_S - \langle \mathcal{C}^{-1}\boldsymbol{\sigma}, \text{grad } \boldsymbol{v} \rangle_S \\
&\quad + \langle \text{grad } \boldsymbol{u}, \text{grad } \boldsymbol{v} \rangle_S \\
&\quad - \langle \text{curl } \boldsymbol{u}, n \rangle_S - \langle \text{curl } \boldsymbol{v}, m \rangle_S \\
&\quad + \langle m\boldsymbol{\chi}, \mathcal{C}^{-1}\boldsymbol{\tau} \rangle_S + \langle \mathcal{C}^{-1}\boldsymbol{\sigma}, n\boldsymbol{\chi} \rangle_S \\
&\quad + 2mn \\
&\quad + \langle \boldsymbol{\pi}, \boldsymbol{\xi} \rangle_F + \langle \text{div } \boldsymbol{\pi}, \text{div } \boldsymbol{\xi} \rangle_F \\
&\quad - \langle \text{grad } p, \boldsymbol{\xi} \rangle_F - \langle \boldsymbol{\pi}, \text{grad } q \rangle_F \\
&\quad + \langle \text{grad } p, \text{grad } q \rangle_F \\
&\quad + \langle \boldsymbol{\sigma}\boldsymbol{\nu}_F, \boldsymbol{\tau}\boldsymbol{\nu}_F \rangle_\Sigma \\
&\quad + \langle p\boldsymbol{\nu}_F, \boldsymbol{\tau}\boldsymbol{\nu}_F \rangle_\Sigma + \langle \boldsymbol{\sigma}\boldsymbol{\nu}_F, q\boldsymbol{\nu}_F \rangle_\Sigma \\
&\quad + \langle \boldsymbol{\pi} \cdot \boldsymbol{\nu}_F, \boldsymbol{\xi} \cdot \boldsymbol{\nu}_F \rangle_\Sigma + \langle p\boldsymbol{\nu}_F, q\boldsymbol{\nu}_F \rangle_\Sigma \\
&= \omega^2 \left(-\langle \rho_S \boldsymbol{u}, \text{div } \boldsymbol{\tau} \rangle_S - \langle \frac{1}{c^2} p, \text{div } \boldsymbol{\xi} \rangle_F + \langle \rho_F \boldsymbol{u} \cdot \boldsymbol{\nu}_F, \boldsymbol{\xi} \cdot \boldsymbol{\nu}_F \rangle_\Sigma \right) .
\end{aligned}
\tag{14}
$$

In what follows we assume that the least-squares functional, variational formulation and eigenvalue problem are defined by equations (12), (13) and (14), respectively.

4.3 Existence and Uniqueness

As already studied in Section 1.4, the necessary condition for existence and uniqueness for the variational formulation (13) is the norm equivalence of the least-squares functional,

$$\alpha_1 \|(\boldsymbol{\tau}, \boldsymbol{v}, n, \boldsymbol{\xi}, q)\|^2_{\mathcal{W}} \leq F(\boldsymbol{\tau}, \boldsymbol{v}, n, \boldsymbol{\xi}, q; \mathbf{0}, 0) \leq \alpha_2 \|(\boldsymbol{\tau}, \boldsymbol{v}, n, \boldsymbol{\xi}, q)\|^2_{\mathcal{W}}$$

for positive α_1 and α_2. In this section we demonstrate this key result by proving ellipticity of the least-squares functional,

$$\alpha_1 \|(\boldsymbol{\tau}, \boldsymbol{v}, n, \boldsymbol{\xi}, q)\|^2_{\mathcal{W}} \leq F(\boldsymbol{\tau}, \boldsymbol{v}, n, \boldsymbol{\xi}, q; \mathbf{0}, 0)$$

and continuity of the least-squares functional

$$F(\boldsymbol{\tau}, \boldsymbol{v}, n, \boldsymbol{\xi}, q; \mathbf{0}, 0) \leq \alpha_2 \|(\boldsymbol{\tau}, \boldsymbol{v}, n, \boldsymbol{\xi}, q)\|^2_{\mathcal{W}}$$

separately in Section 4.3.1 and Section 4.3.2. Following the results of Theorem 4.5 and Theorem 4.6 we will already state the desired theorem:

Theorem 4.1 (Norm equivalence)**.** *There exists positive constants α_1 and α_2 such that the least-squares functional $F(\boldsymbol{\tau}, \boldsymbol{v}, n, \boldsymbol{\xi}, q; \mathbf{0}, 0)$ defined in equation* (12) *is norm equivalent with respect to the norm $\|\cdot\|_{\mathcal{W}}$ defined in equation* (10)*,*

$$\alpha_1 \|(\boldsymbol{\tau}, \boldsymbol{v}, n, \boldsymbol{\xi}, q)\|^2_{\mathcal{W}} \leq F(\boldsymbol{\tau}, \boldsymbol{v}, n, \boldsymbol{\xi}, q; \mathbf{0}, 0) \leq \alpha_2 \|(\boldsymbol{\tau}, \boldsymbol{v}, n, \boldsymbol{\xi}, q)\|^2_{\mathcal{W}} .$$

In the remainder of this chapter we will assume that α is a generic positive constant, possibly different at different occurrences.

4.3.1 Ellipticity

To prove the lower bound of Theorem 4.1 we will split the least-squares functional into terms related to the solid, fluid and interface equations and first provide lower bounds on these functionals individually before concluding the ellipticity result in Theorem 4.5. Therefore, the LS functional $F(\boldsymbol{\tau}, \boldsymbol{v}, n, \boldsymbol{\xi}, q; \mathbf{0}, 0)$ as defined in equation (12) is split into

$$F(\boldsymbol{\tau}, \boldsymbol{v}, n, \boldsymbol{\xi}, q; \mathbf{0}, 0) = F_S(\boldsymbol{\tau}, \boldsymbol{v}, n) + F_F(\boldsymbol{\xi}, q) + F_\Sigma(\boldsymbol{\tau}, \boldsymbol{v}, n, \boldsymbol{\xi}, q)$$

with

$$F_S(\boldsymbol{\tau}, \boldsymbol{v}, n) = \|\mathcal{C}^{-1}\boldsymbol{\tau} - \operatorname{grad} \boldsymbol{v} + n\boldsymbol{\chi}\|_S^2 + \|\operatorname{div} \boldsymbol{\tau}\|_S^2 + \|sk(\boldsymbol{\tau})\|_S^2, \tag{15}$$

$$F_F(\boldsymbol{\xi}, q) = \|\boldsymbol{\xi} - \operatorname{grad} q\|_F^2 + \|\operatorname{div} \boldsymbol{\xi}\|_F^2 \ , \tag{16}$$

$$F_\Sigma(\boldsymbol{\tau}, \boldsymbol{v}, n, \boldsymbol{\xi}, q) = \|\boldsymbol{\tau}\boldsymbol{\nu}_F + q\boldsymbol{\nu}_F\|_\Sigma^2 + \|\boldsymbol{\xi} \cdot \boldsymbol{\nu}_F\|_\Sigma^2 \ . \tag{17}$$

(A lower bound: solid functional) The lower bound of the solid functional (15) is obtained with respect to the norm

$$\|(\boldsymbol{\tau}, \boldsymbol{v}, n)\|_{\mathcal{W}_S}^2 = \|\boldsymbol{\tau}\|_{H(div;\Omega_S)}^2 + \|\boldsymbol{\tau}\boldsymbol{\nu}_F\|_{L^2(\Sigma)}^2 + \|\boldsymbol{v}\|_{H^1(\Omega_S)}^2 + \|n\|_{L^2(\Omega_S)}^2 \ .$$

In order to obtain the ellipticity of the solid functional, we first state some useful results:

Lemma 4.1 (Korn's inequality)**.** Let Ω be an open bounded set in $\mathbb{R}^d$ with piecewise smooth boundary. In addition suppose Γ_0 has positive $(d-1)$-dimensional measure. Then there exists a positive number $\alpha(\Omega, \Gamma_0)$ such that

$$\|\varepsilon(\boldsymbol{v})\|_{L^2(\Omega)}^2 \geq \alpha \|\boldsymbol{v}\|_{H^1(\Omega)}^2 \text{ for all } \boldsymbol{v} \in H^1_{\Gamma_0}(\Omega)^d$$

where $\varepsilon(\boldsymbol{v})$ is the symmetric strain tensor.

Proof. See, e.g. [8, VI.3]. □

Lemma 4.2 (Stress Tensor Bound)**.** For $\boldsymbol{\tau} \in H(div; \Omega_S)$, there exist a positive constant α such that

$$\|\boldsymbol{\tau}\|_S^2 \leq \alpha \left(\|dev(\boldsymbol{\tau})\|_S^2 + \|\operatorname{div} \boldsymbol{\tau}\|_S^2 \right)$$

with the deviatoric stress $dev(\boldsymbol{\tau}) \coloneqq \frac{1}{2\mu} \left(\boldsymbol{\tau} - \frac{1}{2} tr(\boldsymbol{\tau}) \boldsymbol{\delta} \right)$.

Proof. The proof is given in [11, Lemma 3.2]. □

The ellipticity result for the solid functional then reads:

Theorem 4.2 (Ellipticity of the Solid Functional)**.** *There exists a positive constant α such that*

$$\|(\boldsymbol{\tau}, \boldsymbol{v}, n)\|_{\mathcal{W}_S}^2 \leq \alpha \left(F_S(\boldsymbol{\tau}, \boldsymbol{v}, n) + \langle \boldsymbol{\tau}\boldsymbol{\nu}_S, \boldsymbol{v} \rangle_\Sigma \right) + \|\boldsymbol{\tau}\boldsymbol{\nu}_F\|_\Sigma^2 \ .$$

Proof. We first notice that $\varepsilon(\boldsymbol{v})$, $\boldsymbol{\delta}$ and $\boldsymbol{\chi}$ are symmetric and skew-symmetric tensors, respectively. Furthermore, we recall $\mathcal{C}^{-1}\boldsymbol{\tau} = \frac{1}{2\mu}\left(\boldsymbol{\tau} - \frac{\lambda}{2\lambda+2\mu} tr(\boldsymbol{\tau})\boldsymbol{\delta}\right)$. One can hence rewrite

$$\begin{aligned}
\langle \mathcal{C}^{-1}\boldsymbol{\tau}, \varepsilon(\boldsymbol{v})\rangle_S &= \langle sym(\mathcal{C}^{-1}\boldsymbol{\tau}), \text{grad } \boldsymbol{v}\rangle_S \\
&= \frac{1}{2\mu}\left(\langle \boldsymbol{\tau}, \text{grad } \boldsymbol{v}\rangle_S - \langle sk(\boldsymbol{\tau}), \text{grad } \boldsymbol{v}\rangle_S + \frac{\lambda}{2\mu+2\lambda}\langle tr(\boldsymbol{\tau})\boldsymbol{\delta}, \text{grad } \boldsymbol{v}\rangle_S\right) \\
&= \frac{1}{2\mu}\left(-\langle \text{div } \boldsymbol{\tau}, \boldsymbol{v}\rangle_S - \langle sk(\boldsymbol{\tau}), \text{grad } \boldsymbol{v}\rangle_S + \frac{\lambda}{2\mu+2\lambda}\langle tr(\boldsymbol{\tau})\delta, \text{grad } \boldsymbol{v}\rangle_S\right) \\
&\quad + \frac{1}{2\mu}\langle \boldsymbol{\tau}\boldsymbol{\nu}_S, \boldsymbol{v}\rangle_\Sigma \ ,
\end{aligned}$$

where we used integration by parts and applied the prescribed boundary conditions on Γ_D and Γ_N. Furthermore we conclude

$$\langle n\boldsymbol{\chi}, \varepsilon(\boldsymbol{v})\rangle_S = 0 \quad \text{and} \quad \langle n\boldsymbol{\chi}, \mathcal{C}^{-1}\boldsymbol{\tau}\rangle_S = \frac{1}{2\mu}\langle n\boldsymbol{\chi}, sk(\boldsymbol{\tau})\rangle_S \ .$$

The norm of $\varepsilon(\boldsymbol{v})$ can now be rewritten to

$$\begin{aligned}
\|\varepsilon(\boldsymbol{v})\|_S^2 &= \langle \text{grad } \boldsymbol{v}, \varepsilon(\boldsymbol{v})\rangle_S \\
&= \langle -\mathcal{C}^{-1}\boldsymbol{\tau} - n\boldsymbol{\chi} + \text{grad } \boldsymbol{v}, \varepsilon(\boldsymbol{v})\rangle_S + \langle \mathcal{C}^{-1}\boldsymbol{\tau}, \varepsilon(\boldsymbol{v})\rangle_S \\
&= \langle -\mathcal{C}^{-1}\boldsymbol{\tau} - n\boldsymbol{\chi} + \text{grad } \boldsymbol{v}, \varepsilon(\boldsymbol{v})\rangle_S \\
&\quad + \frac{1}{2\mu}\left(-\langle \text{div } \boldsymbol{\tau}, \boldsymbol{v}\rangle_S - \langle sk(\boldsymbol{\tau}), \text{grad } \boldsymbol{v}\rangle_S + \frac{\lambda}{2\mu+2\lambda}\langle tr(\boldsymbol{\tau})\boldsymbol{\delta}, \text{grad } \boldsymbol{v}\rangle_S\right) \\
&\quad + \frac{1}{2\mu}\langle \boldsymbol{\tau}\boldsymbol{\nu}_S, \boldsymbol{v}\rangle_\Sigma \ .
\end{aligned} \tag{18}$$

We furthermore observe

$$\begin{aligned}
\frac{\lambda}{4\mu(2\lambda+2\mu)^2}\|tr(\boldsymbol{\tau})\boldsymbol{\delta}\|_S^2 &= \langle \frac{1}{2\mu}\frac{\lambda}{2\mu+2\lambda} tr(\boldsymbol{\tau})\boldsymbol{\delta}, \frac{1}{2}\frac{1}{2\mu+2\lambda} tr(\boldsymbol{\tau})\boldsymbol{\delta} - dev(\boldsymbol{\tau}) - n\boldsymbol{\chi}\rangle_S \\
&= \langle \frac{1}{2\mu}\frac{\lambda}{2\mu+2\lambda} tr(\boldsymbol{\tau})\boldsymbol{\delta}, -\mathcal{C}^{-1}\boldsymbol{\tau} - n\boldsymbol{\chi}\rangle_S
\end{aligned} \tag{19}$$

where $dev(\boldsymbol{\tau})$ denotes the deviatoric part of the stress tensor defined by $dev(\boldsymbol{\tau}) = \frac{1}{2\mu}\left(\boldsymbol{\tau} - \frac{1}{2}tr(\boldsymbol{\tau})\boldsymbol{\delta}\right)$. By simple calculations one can observe

$$\langle dev(\boldsymbol{\tau}), \boldsymbol{\delta}\rangle_S = 0 \quad \text{and} \quad \mathcal{C}^{-1}\boldsymbol{\tau} = dev(\boldsymbol{\tau}) + \frac{1}{2}\frac{1}{2\mu+2\lambda} tr(\boldsymbol{\tau})\boldsymbol{\delta}$$

which proves equation (19). Then, it follows from equation (18) together with equation (19)

$$\begin{aligned}
\|\varepsilon(\boldsymbol{v})\|_S^2 &\leq \|\varepsilon(\boldsymbol{v})\|_S^2 + \frac{\lambda}{4\mu(2\lambda+2\mu)^2}\|tr(\boldsymbol{\tau})\boldsymbol{\delta}\|_S^2 \\
&= \langle -\mathcal{C}^{-1}\boldsymbol{\tau} - n\boldsymbol{\chi} + \text{grad } \boldsymbol{v}, \varepsilon(\boldsymbol{v})\rangle_S \\
&\quad + \frac{1}{2\mu}\left(-\langle \text{div } \boldsymbol{\tau}, \boldsymbol{v}\rangle_S - \langle sk(\boldsymbol{\tau}), \text{grad } \boldsymbol{v}\rangle_S + \frac{\lambda}{2\mu+2\lambda}\langle tr(\boldsymbol{\tau})\boldsymbol{\delta}, \text{grad } \boldsymbol{v}\rangle_S\right) \\
&\quad + \frac{1}{2\mu}\frac{\lambda}{2\mu+2\lambda}\langle tr(\boldsymbol{\tau})\boldsymbol{\delta}, -\mathcal{C}^{-1}\boldsymbol{\tau} - n\boldsymbol{\chi}\rangle_S + \frac{1}{2\mu}\langle \boldsymbol{\tau}\boldsymbol{\nu}_S, \boldsymbol{v}\rangle_\Sigma \\
&\leq \Big|\langle -\mathcal{C}^{-1}\boldsymbol{\tau} - n\boldsymbol{\chi} + \text{grad } \boldsymbol{v}, \varepsilon(\boldsymbol{v})\rangle_S \\
&\quad + \frac{1}{2\mu}\left(-\langle \text{div } \boldsymbol{\tau}, \boldsymbol{v}\rangle_S - \langle sk(\boldsymbol{\tau}), \text{grad } \boldsymbol{v}\rangle_S + \frac{\lambda}{2\mu+2\lambda}\langle tr(\boldsymbol{\tau})\boldsymbol{\delta}, \text{grad } \boldsymbol{v} - \mathcal{C}^{-1}\boldsymbol{\tau} - n\boldsymbol{\chi}\rangle_S\right)\Big| \\
&\quad + \frac{1}{2\mu}\langle \boldsymbol{\tau}\boldsymbol{\nu}_S, \boldsymbol{v}\rangle_\Sigma \\
&\leq \alpha\left(\|-\mathcal{C}^{-1}\boldsymbol{\tau} - n\boldsymbol{\chi} + \text{grad } \boldsymbol{v}\|_S\|\varepsilon(\boldsymbol{v})\|_S + \|\text{div } \boldsymbol{\tau}\|_S\|\boldsymbol{v}\|_S + \|sk(\boldsymbol{\tau})\|_S\|\text{grad } \boldsymbol{v}\|_S\right. \\
&\quad \left.+\|-\mathcal{C}^{-1}\boldsymbol{\tau} - n\boldsymbol{\chi} + \text{grad } \boldsymbol{v}\|_S\|tr(\boldsymbol{\tau})\boldsymbol{\delta}\|_S\right) + \frac{1}{2\mu}\langle \boldsymbol{\tau}\boldsymbol{\nu}_S, \boldsymbol{v}\rangle_\Sigma \\
&\leq \alpha F(\boldsymbol{\tau}, \boldsymbol{v}, n)^{\frac{1}{2}}\left(\|\varepsilon(\boldsymbol{v})\|_S + \|tr(\boldsymbol{\tau})\boldsymbol{\delta}\|_S\right) + \frac{1}{2\mu}\langle \boldsymbol{\tau}\boldsymbol{\nu}_S, \boldsymbol{v}\rangle_\Sigma\ , \qquad (20)
\end{aligned}$$

where the triangle inequality and Cauchy-Schwarz inequality are used in the second to last line and Korn's inquality is applied in the last line.
The bound of $\|n\boldsymbol{\chi}\|_S^2$ is obtained by observing

$$\begin{aligned}
\|n\boldsymbol{\chi}\|_S^2 &\leq \left|\langle \mathcal{C}^{-1}\boldsymbol{\tau} + n\boldsymbol{\chi} - \text{grad } \boldsymbol{v}, n\boldsymbol{\chi}\rangle_S - \frac{1}{2\mu}\langle sk(\boldsymbol{\tau}), n\boldsymbol{\chi}\rangle_S + \langle \text{grad } \boldsymbol{v}, n\boldsymbol{\chi}\rangle_S\right| \\
&\leq \|\mathcal{C}^{-1}\boldsymbol{\tau} + n\boldsymbol{\chi} - \text{grad } \boldsymbol{v}\|_S\|n\boldsymbol{\chi}\|_S + \frac{1}{2\mu}\|sk(\boldsymbol{\tau})\|_S\|n\boldsymbol{\chi}\|_S + \|\text{grad } \boldsymbol{v}\|_S\|n\boldsymbol{\chi}\|_S \\
&\leq \alpha\left(F(\boldsymbol{\tau}, \boldsymbol{v}, n)^{\frac{1}{2}} + \|\text{grad } \boldsymbol{v}\|_S\right)\|n\boldsymbol{\chi}\|_S \\
&\leq \alpha\left(F(\boldsymbol{\tau}, \boldsymbol{v}, n)^{\frac{1}{2}} + \|\varepsilon(\boldsymbol{v})\|_S\right)\|n\boldsymbol{\chi}\|_S\ ,
\end{aligned}$$

where a triangle inequality, a Cauchy-Schwarz inequality and Korn's inquality were applied consecutively. One can conclude

$$\|n\boldsymbol{\chi}\|_S \leq \alpha\left(F(\boldsymbol{\tau}, \boldsymbol{v}, n)^{\frac{1}{2}} + \|\varepsilon(\boldsymbol{v})\|_S\right)\ . \qquad (21)$$

We furthermore note

$$\begin{aligned}
\|dev(\boldsymbol{\tau})\|_S^2 &= \frac{1}{2\mu}\langle \boldsymbol{\tau}, dev(\boldsymbol{\tau})\rangle_S \\
&= \langle \mathcal{C}^{-1}\boldsymbol{\tau} + n\boldsymbol{\chi} - \text{grad } \boldsymbol{v}, dev(\boldsymbol{\tau})\rangle_S - \langle n\boldsymbol{\chi}, dev(\boldsymbol{\tau})\rangle_S + \langle \text{grad } \boldsymbol{v}, dev(\boldsymbol{\tau})\rangle_S \\
&\leq \alpha\left(F(\boldsymbol{\tau}, \boldsymbol{v}, n)^{\frac{1}{2}} + \|\varepsilon(\boldsymbol{v})\|_S + \|n\boldsymbol{\chi}\|_S\right)\|dev(\boldsymbol{\tau})\|_S \\
&\leq \alpha\left(F(\boldsymbol{\tau}, \boldsymbol{v}, n)^{\frac{1}{2}} + \|\varepsilon(\boldsymbol{v})\|_S\right)\|dev(\boldsymbol{\tau})\|_S
\end{aligned}$$

where we substituted equation (21) in the last inequality. We can conclude

$$\|dev(\boldsymbol{\tau})\|_S \leq \alpha\left(F(\boldsymbol{\tau}, \boldsymbol{v}, n)^{\frac{1}{2}} + \|\varepsilon(\boldsymbol{v})\|_S\right)\ .$$

Employing the results of Lemma 4.2 combined with the above inequality yields the result

$$\begin{aligned}\|\boldsymbol{\tau}\|_S &\leq \|dev(\boldsymbol{\tau})\|_S + \|\text{div } \boldsymbol{\tau}\|_S \\ &\leq \alpha \left(F(\boldsymbol{\tau}, \boldsymbol{v}, n)^{\frac{1}{2}} + \|\varepsilon(\boldsymbol{v})\|_S \right) \ . \end{aligned} \tag{22}$$

What remains is to find an upper bound for $\|tr(\boldsymbol{\tau})\boldsymbol{\delta}\|_S$. This is readily done by rewriting

$$\begin{aligned}\|tr(\boldsymbol{\tau})\boldsymbol{\delta}\|_S^2 &= |\langle tr(\boldsymbol{\tau})\boldsymbol{\delta}, tr(\boldsymbol{\tau})\boldsymbol{\delta}\rangle_S| = 2\,|\langle tr(\boldsymbol{\tau})\boldsymbol{\delta}, \boldsymbol{\tau}\rangle_S| \\ &\leq 2\|tr(\boldsymbol{\tau})\boldsymbol{\delta}\|_S \|\boldsymbol{\tau}\|_S \ , \end{aligned}$$

employing the Cauchy-Schwarz inequality, yielding the upper bound

$$\|tr(\boldsymbol{\tau})\boldsymbol{\delta}\|_S \leq 2\|\boldsymbol{\tau}\|_S \ . \tag{23}$$

Together with equation (22) we conclude

$$\|tr(\boldsymbol{\tau})\boldsymbol{\delta}\|_S \leq \alpha \left(F(\boldsymbol{\tau}, \boldsymbol{v}, n)^{\frac{1}{2}} + \|\varepsilon(\boldsymbol{v})\|_S \right) \ . \tag{24}$$

Combining equation (20) and equation (24), for all $\gamma > 0$ yields

$$\begin{aligned}\|\varepsilon(\boldsymbol{v})\|_S^2 &\leq \alpha F(\boldsymbol{\tau}, \boldsymbol{v}, n)^{\frac{1}{2}} \left(F(\boldsymbol{\tau}, \boldsymbol{v}, n)^{\frac{1}{2}} + \|\varepsilon(\boldsymbol{v})\|_S \right) + \frac{1}{2\mu}\langle \boldsymbol{\tau}\boldsymbol{\nu}_S, \boldsymbol{v}\rangle_\Sigma \\ &\leq \frac{\gamma\alpha^2 F(\boldsymbol{\tau}, \boldsymbol{v}, n)}{2} + \frac{(F(\boldsymbol{\tau}, \boldsymbol{v}, n)^{\frac{1}{2}} + \|\varepsilon(\boldsymbol{v})\|_S)^2}{2\gamma} + \frac{1}{2\mu}\langle \boldsymbol{\tau}\boldsymbol{\nu}_S, \boldsymbol{v}\rangle_\Sigma \\ &\leq \frac{\gamma\alpha^2 F(\boldsymbol{\tau}, \boldsymbol{v}, n)}{2} + \frac{F(\boldsymbol{\tau}, \boldsymbol{v}, n) + \|\varepsilon(\boldsymbol{v})\|_S^2}{\gamma} + \frac{1}{2\mu}\langle \boldsymbol{\tau}\boldsymbol{\nu}_S, \boldsymbol{v}\rangle_\Sigma \ , \end{aligned}$$

where we used the ϵ-inequality with $\gamma > 0$ in the second line. Choosing $\gamma > 0$ sufficiently large yields the upper bound

$$\|\varepsilon(\boldsymbol{v})\|_S^2 \leq \alpha F(\boldsymbol{\tau}, \boldsymbol{v}, n) + \frac{1}{2\mu}\langle \boldsymbol{\tau}\boldsymbol{\nu}_S, \boldsymbol{v}\rangle_\Sigma \tag{25}$$

Combining equations (25), (22) and (21) we obtain the desired result

$$\begin{aligned}\|(\boldsymbol{\tau}, \boldsymbol{v}, n)\|_{\mathcal{W}_S}^2 &\leq \alpha \left(\|\boldsymbol{\tau}\|_S^2 + \|\text{div } \boldsymbol{\tau}\|_S^2 + \|\varepsilon(\boldsymbol{v})\|_S^2 + \|n\boldsymbol{\chi}\|_S^2 \right) + \|\boldsymbol{\tau}\boldsymbol{\nu}_F\|_\Sigma^2 \\ &\leq \alpha \left(F(\boldsymbol{\tau}, \boldsymbol{v}, n) + \langle \boldsymbol{\tau}\boldsymbol{\nu}_S, \boldsymbol{v}\rangle_\Sigma \right) + \|\boldsymbol{\tau}\boldsymbol{\nu}_F\|_\Sigma^2 \ . \end{aligned}$$

□

(A lower bound: fluid functional) A lower bound for the fluid functional $F_F(\boldsymbol{\xi}, q)$ is given with the corresponding norm

$$\|(\boldsymbol{\xi}, q)\|_{\mathcal{W}_F}^2 = \|\boldsymbol{\xi}\|_{H(div;\Omega_F)}^2 + \|\boldsymbol{\xi}\cdot\boldsymbol{\nu}_F\|_\Sigma^2 + \|q\|_{H^1(\Omega_F)}^2 \ .$$

Before stating the ellipticity result we first recall an inequality of Poincaré-Friedrichs type of the following form:

Lemma 4.3 (Inequality of Poincaré-Friedrichs type)**.** Let Ω be a bounded connected open set with Lipschitz boundary. Then, there there is a $\alpha(\Omega) > 0$ such that

$$\|q\|_{H^1(\Omega)}^2 \leq \alpha \left(\frac{1}{|\partial\Omega|} \left(\int_{\partial\Omega} q \ d\Gamma \right)^2 + \|\text{grad } q\|_{L^2(\Omega)}^2 \right)$$

Proof. This theorem is a consequence of [13, Lemma B.63] and [13, Example B.64]. □

Theorem 4.3 (Ellipticity of the Fluid Functional)**.** *There exists a positive constant* α *such that*

$$\|(\boldsymbol{\xi}, q)\|^2_{\mathcal{W}_F} \leq \alpha \left(F_F(\boldsymbol{\xi}, q) + \langle \boldsymbol{\xi} \cdot \boldsymbol{\nu}_F, q \rangle_{L^2(\Sigma)} + \frac{1}{|\Sigma|} \left(\int_\Sigma q \, d\Gamma \right)^2 \right) + \|\boldsymbol{\xi} \cdot \boldsymbol{\nu}_F\|^2_\Sigma \ .$$

Proof. We start by rewriting

$$\begin{aligned} \alpha \left(F_F(\boldsymbol{\xi}, q) + \frac{1}{|\Sigma|} \left(\int_\Sigma q \, d\Gamma \right)^2 \right) &\geq \|\boldsymbol{\xi}\|^2_F + \|\text{grad } q\|^2_F + 2\gamma \|\text{div } \boldsymbol{\xi}\|^2_F \\ &\quad - 2\langle \boldsymbol{\xi}, \text{grad } q \rangle_F + \frac{1}{|\Sigma|} \left(\int_\Sigma q \, d\Gamma \right)^2 \\ &\geq \|\boldsymbol{\xi}\|^2_F + \alpha_P \|q\|^2_{H^1(\Omega_F)} + 2\gamma \|\text{div } \boldsymbol{\xi}\|^2_F + 2\langle \text{div } \boldsymbol{\xi}, q \rangle_F - 2\langle \boldsymbol{\xi} \cdot \boldsymbol{\nu}_F, q \rangle_\Sigma \\ &\geq \|\boldsymbol{\xi}\|^2_F + \gamma \|\text{div } \boldsymbol{\xi}\|^2_F + \alpha_P \|q\|^2_{H^1(\Omega_F)} - \frac{1}{\gamma} \|q\|^2_F - 2\langle \boldsymbol{\xi} \cdot \boldsymbol{\nu}_F, q \rangle_\Sigma \ , \end{aligned}$$

for all $\gamma > 0$ and fixed α_P originating from the Poincaré-Friedrichs inequality. This yields the required result for γ sufficiently large. □

(A lower bound: interface functional) As a last steps towards the ellipticity result we bound the interface terms of the least-squares functional in the following way:

Theorem 4.4 (Ellipticity of the Interface Functional)**.** *There exists positive constants* $0 < \alpha_1$, $0 < \alpha_2 < 1$ *such that*

$$\begin{aligned} \alpha_1 F_\Sigma(\boldsymbol{\tau}, \boldsymbol{v}, n, \boldsymbol{\xi}, q) \geq \langle \boldsymbol{\tau}\boldsymbol{\nu}_F, \boldsymbol{v} \rangle_\Sigma + \langle \boldsymbol{\xi} \cdot \boldsymbol{\nu}_F, q \rangle_\Sigma + \frac{1}{|\Sigma|} \left(\int_\Sigma q \, d\Gamma \right)^2 + \|\boldsymbol{\tau}\boldsymbol{\nu}_F\|^2_\Sigma + \|\boldsymbol{\xi} \cdot \boldsymbol{\nu}_F\|^2_\Sigma \\ - \alpha_2 \|\boldsymbol{\tau}\boldsymbol{\nu}_F\|^2_\Sigma - \alpha_2 \|\boldsymbol{v}\|^2_{H^1(\Omega_S)} - \alpha_2 \|q\|^2_{H^1(\Omega_F)} \ . \end{aligned}$$

Proof. We start by obtaining a bound for the boundary-integral term

$$\frac{1}{|\Sigma|} \left(\int_\Sigma q \, d\Gamma \right)^2 \leq \frac{1}{|\Sigma|} \left(\int_\Sigma |q| \, d\Gamma \right)^2 \leq \|q\|^2_{L^2(\Sigma)} \ ,$$

where the last inequality is obtained directly by Hölders inequality. We can bound the least-squares functional by

$$(2 + \frac{1}{\alpha}) F_\Sigma(\boldsymbol{\tau}, \boldsymbol{v}, n, \boldsymbol{\xi}, q) \geq (2 + \frac{1}{\alpha}) \|\boldsymbol{\tau}\boldsymbol{\nu}_F + q\boldsymbol{\nu}_F\|^2_\Sigma + (1 + \frac{1}{\alpha}) \|\boldsymbol{\xi} \cdot \boldsymbol{\nu}_F\|^2_\Sigma$$

for any $\alpha > 0$. Using

$$\begin{aligned} \frac{1}{\alpha} \|\boldsymbol{\tau}\boldsymbol{\nu}_F + q\boldsymbol{\nu}_F\|^2_\Sigma \geq -\alpha\rho^2 \|\boldsymbol{v}\|^2_\Sigma + 2\rho \langle \boldsymbol{v}, \boldsymbol{\tau}\boldsymbol{\nu}_F + q\boldsymbol{\nu}_F \rangle_\Sigma \quad \text{and} \\ \frac{1}{\alpha} \|\boldsymbol{\xi} \cdot \boldsymbol{\nu}_F\|^2_\Sigma \geq -\alpha \|q\|^2_\Sigma + 2\langle \boldsymbol{\xi} \cdot \boldsymbol{\nu}_F, q \rangle_\Sigma \end{aligned}$$

for $\rho > 0$, one can now split the least-squares functional into

$$\begin{aligned}(2+\frac{1}{\alpha})F_\Sigma(\boldsymbol{\tau},\boldsymbol{v},n,\boldsymbol{\xi},q) \geq\ & 2\|\boldsymbol{\tau}\boldsymbol{\nu}_F\|_\Sigma^2 + 2\|q\boldsymbol{\nu}_F\|_\Sigma^2 + 4\langle\boldsymbol{\tau}\boldsymbol{\nu}_F, q\boldsymbol{\nu}_F\rangle_\Sigma + \|\boldsymbol{\xi}\cdot\boldsymbol{\nu}_F\|_\Sigma^2 \\ & - \alpha\rho^2\|v\|_\Sigma^2 + 2\rho\langle\boldsymbol{\tau}\boldsymbol{\nu}_F,\boldsymbol{v}\rangle_\Sigma + 2\rho\langle q\boldsymbol{\nu}_F,\boldsymbol{v}\rangle_\Sigma \\ & - \alpha\|q\|_\Sigma^2 + 2\langle\boldsymbol{\xi}\cdot\boldsymbol{\nu}_F, q\rangle_\Sigma\ .\end{aligned}$$

Furthermore, we observe

$$\begin{aligned}2\langle q\boldsymbol{\nu}_F, 2\boldsymbol{\tau}\boldsymbol{\nu}_F + \rho\boldsymbol{v}\rangle_\Sigma &\geq -\beta\|2\boldsymbol{\tau}\boldsymbol{\nu}_F + \rho\boldsymbol{v}\|_\Sigma^2 - \frac{1}{\beta}\|q\boldsymbol{\nu}_F\|_\Sigma^2 \\ &\geq -4\beta\|\boldsymbol{\tau}\boldsymbol{\nu}_F\|_\Sigma^2 - \beta\rho^2\|\boldsymbol{v}\|_\Sigma^2 - 4\beta\rho\langle\boldsymbol{\tau}\boldsymbol{\nu}_F,\boldsymbol{v}\rangle_\Sigma - \frac{1}{\beta}\|q\boldsymbol{\nu}_F\|_\Sigma^2\end{aligned}$$

for $\beta > 0$ and obtain

$$\begin{aligned}(2+\frac{1}{\alpha})F_\Sigma(\boldsymbol{\tau},\boldsymbol{v},n,\boldsymbol{\xi},q) \geq\ & (2-4\beta)\|\boldsymbol{\tau}\boldsymbol{\nu}_F\|_\Sigma^2 + (2-\frac{1}{\beta})\|q\boldsymbol{\nu}_F\|_\Sigma^2 - \beta\rho^2\|v\|_\Sigma^2 + \|\boldsymbol{\xi}\cdot\boldsymbol{\nu}_F\|_\Sigma^2 \\ & + (2-4\beta\rho)\langle\boldsymbol{\tau}\boldsymbol{\nu}_F,\boldsymbol{v}\rangle_\Sigma - \alpha\rho^2\|\boldsymbol{v}\|_\Sigma^2 - \alpha\|q\|_\Sigma^2 + 2\langle\boldsymbol{\xi}\cdot\boldsymbol{\nu}_F, q\rangle_\Sigma\ .\end{aligned}$$

After reordering the terms and substituting $\|q\boldsymbol{\nu}_F\|_\Sigma^2 = \|q\|_\Sigma^2$ we obtain the estimate

$$\begin{aligned}(2+\frac{1}{\alpha})F_\Sigma(\boldsymbol{\tau},\boldsymbol{v},n,\boldsymbol{\xi},q) \geq\ & (2-4\beta)\|\boldsymbol{\tau}\boldsymbol{\nu}_F\|_\Sigma^2 + \rho^2(-\beta-\alpha)\|v\|_\Sigma^2 + (2-\frac{1}{\beta}-\alpha)\|q\|_\Sigma^2 + \|\boldsymbol{\xi}\cdot\boldsymbol{\nu}_F\|_\Sigma^2 \\ & + (2-4\beta\rho)\langle\boldsymbol{\tau}\boldsymbol{\nu}_F,\boldsymbol{v}\rangle_\Sigma + 2\langle\boldsymbol{\xi}\cdot\boldsymbol{\nu}_F, q\rangle_\Sigma\ .\end{aligned}$$

Upper bounds for $\|q\|_{L^2(\Sigma)}^2$ and $\|\boldsymbol{v}\|_{L^2(\Sigma)}^2$ can be obtained using standard trace theorems (see, for example, [14, Chapter 5.5]),

$$\begin{aligned}\|q\|_{L^2(\Sigma)}^2 &\leq \gamma_T\|q\|_{H^1(\Omega_F)}^2, \\ \|\boldsymbol{v}\|_{L^2(\Sigma)}^2 &\leq \gamma_T\|\boldsymbol{v}\|_{H^1(\Omega_S)}^2\end{aligned}$$

for some $\gamma_T > 0$. Now observe that we can split $(2-\frac{1}{\beta}-\alpha)\|q\|_\Sigma^2$ into

$$(2-\frac{1}{\beta}-\alpha)\|q\|_\Sigma^2 = (2-\frac{1-\kappa}{\beta}-\alpha)\|q\|_\Sigma^2 - \frac{\kappa}{\beta}\|q\|_\Sigma^2$$

for $0 < \kappa < 1$. Applying the trace theorem only to the latter term yields the estimate

$$\begin{aligned}(2+\frac{1}{\alpha})F_\Sigma(\boldsymbol{\tau},\boldsymbol{v},n,\boldsymbol{\xi},q) \geq\ & (2-4\beta)\|\boldsymbol{\tau}\boldsymbol{\nu}_F\|_\Sigma^2 - \gamma_T\rho^2(\beta+\alpha)\|\boldsymbol{v}\|_{H^1(\Omega_S)}^2 + (2-\frac{1-\kappa}{\beta}-\alpha)\|q\|_\Sigma^2 \\ & - \frac{\kappa\gamma_T}{\beta}\|q\|_{H^1(\Omega_F)}^2 + \|\boldsymbol{\xi}\cdot\boldsymbol{\nu}_F\|_\Sigma^2 + (2-4\beta\rho)\langle\boldsymbol{\tau}\boldsymbol{\nu}_F,\boldsymbol{v}\rangle_\Sigma + 2\langle\boldsymbol{\xi}\cdot\boldsymbol{\nu}_F, q\rangle_\Sigma\ .\end{aligned}$$

To finish the proof we fix $\kappa = \kappa_T$ with $0 < \kappa_T < \frac{\beta}{\gamma_T}$. We furthermore require $(2-\frac{1-\kappa_T}{\beta}-\alpha) > 0$ and $(2-4\beta) > 0$. This is satisfied for $\frac{1-\kappa_T}{2} < \beta < \frac{1}{2}$ and $\alpha < \frac{\kappa_T}{\beta}$. Choosing $\rho < \min\{1, \sqrt{\frac{1}{\gamma_T(\alpha+\beta)}}\}$ ensures $2-4\beta\rho > 0$ and $\gamma_T\rho^2(\alpha+\beta) < 1$. □

(Ellipticity results) What remains is to combine the lower bounds for the solid functional, the fluid functional, and the interface functional into the desired ellipticity result:

Theorem 4.5 (Ellipticity of the Least-Squares Functional)**.** *There exists a positive constant α such that*

$$\|(\boldsymbol{\tau}, \boldsymbol{v}, n, \boldsymbol{\xi}, q)\|_{\mathcal{W}}^2 \leq \alpha F(\boldsymbol{\tau}, \boldsymbol{v}, n, \boldsymbol{\xi}, q) \ .$$

Proof. Combining Theorem 4.2, 4.3 and 4.4 yields an upper bound of the form

$$\begin{aligned}\|(\boldsymbol{\tau}, \boldsymbol{v}, n, \boldsymbol{\xi}, q)\|_{\mathcal{W}}^2 &\leq \beta \left(F_S(\boldsymbol{\tau}, \boldsymbol{v}, n) + F_F(\boldsymbol{\xi}, q) + \langle \boldsymbol{\tau}\boldsymbol{\nu}_S, \boldsymbol{v}\rangle_\Sigma + \langle \boldsymbol{\xi}\cdot\boldsymbol{\nu}_F, q\rangle_\Sigma\right) + \frac{1}{|\Sigma|}\left(\int_{\Omega_F} q \ d\Gamma\right)^2 \\ &\quad + \|\boldsymbol{\tau}\boldsymbol{\nu}_F\|_\Sigma^2 + \|\boldsymbol{\xi}\cdot\boldsymbol{\nu}_F\|_\Sigma^2 \\ &\leq \beta \left(F_S(\boldsymbol{\tau}, \boldsymbol{v}, n) + F_F(\boldsymbol{\xi}, q) + F_\Sigma(\boldsymbol{\tau}, \boldsymbol{v}, n, \boldsymbol{\xi}, q)\right) \\ &\quad + \alpha\|\boldsymbol{\tau}\boldsymbol{\nu}_F\|_\Sigma^2 + \alpha\|v\|_{H^1(\Omega_S)}^2 + \alpha\|q\|_{H^1(\Omega_F)}^2\end{aligned}$$

with $0 < \alpha < 1$ and $\beta > 0$. Reordering the terms and scaling the inequality yields the desired result. □

4.3.2 Continuity

The continuity of the LS functional follows from a more straightforward manner than the ellipticity of the functional. We prove continuity of the functional by rewriting the terms.

Theorem 4.6 (Continuity of the Least-Squares Functional)**.** *There exists a positive constant α such that*

$$\|(\boldsymbol{\tau}, \boldsymbol{v}, n, \boldsymbol{\xi}, q)\|_{\mathcal{W}}^2 \geq \alpha F(\boldsymbol{\tau}, \boldsymbol{v}, n, \boldsymbol{\xi}, q) \ .$$

Proof. One starts by bounding the LS functional by

$$\begin{aligned}F(\boldsymbol{\tau}, \boldsymbol{v}, n, \boldsymbol{\xi}, q) \leq \ &\|\mathcal{C}^{-1}\boldsymbol{\tau}\|_S^2 + \|\text{grad } \boldsymbol{v}\|_S^2 + \|n\boldsymbol{\chi}\|_S^2 + \|\text{div } \boldsymbol{\tau}\|_S^2 + \|sk(\boldsymbol{\tau})\|_S^2 \\ &+ \|\boldsymbol{\xi}\|_F^2 + \|\text{grad } q\|_F^2 + \|\text{div } \boldsymbol{\xi}\|_F^2 \\ &+ \|\boldsymbol{\tau}\boldsymbol{\nu}_F\|_\Sigma^2 + \|q\boldsymbol{\nu}_F\|_\Sigma^2 + \|\boldsymbol{\xi}\cdot\boldsymbol{\nu}_F\|_\Sigma^2 \ .\end{aligned}$$

It remains to bound each term individually. Firstly,

$$\|\mathcal{C}^{-1}\boldsymbol{\tau}\|_S^2 \leq \frac{1}{(2\lambda)^2}\|\boldsymbol{\tau}\|_S^2 + \frac{1}{(2\lambda)^2}\frac{\lambda^2}{(2\lambda+2\lambda)^2}\|tr(\boldsymbol{\tau})\boldsymbol{\delta}\|_S^2 \ ,$$

which together with the bound given in equation (23) yields

$$\|\mathcal{C}^{-1}\boldsymbol{\tau}\|_S^2 \lesssim \|\boldsymbol{\tau}\|_S^2 \ .$$

Furthermore, one can rewrite

$$\|sk(\boldsymbol{\tau})\|_S^2 \leq \|sk(\boldsymbol{\tau})\|_S^2 + \|sym(\boldsymbol{\tau})\|_S^2 = \|\boldsymbol{\tau}\|_S^2 \quad \text{and} \quad \|n\boldsymbol{\chi}\|_S^2 = 2\|n\|_S^2 \ .$$

$$\begin{aligned}F(\boldsymbol{\tau}, \boldsymbol{v}, n, \boldsymbol{\xi}, q) \lesssim \ &\|\boldsymbol{\tau}\|_S^2 + \|\text{grad } \boldsymbol{v}\|_S^2 + \|n\|_S^2 + \|\text{div } \boldsymbol{\tau}\|_S^2 \\ &+ \|\boldsymbol{\xi}\|_F^2 + \|\text{grad } q\|_F^2 + \|\text{div } \boldsymbol{\xi}\|_F^2 \\ &+ \|\boldsymbol{\tau}\boldsymbol{\nu}_F\|_\Sigma^2 + \|q\|_\Sigma^2 + \|\boldsymbol{\xi}\cdot\boldsymbol{\nu}_F\|_\Sigma^2 \ .\end{aligned}$$

Lastly, applying a standard trace theorem as in the precious section

$$\|q\|_{L^2(\Sigma)}^2 \leq \gamma_T\|q\|_{H^1(\Omega_F)}^2$$

concludes the proof after substituting each of the above terms. □

Proving the continuity of the least squares functional concludes the proof of Theorem 4.1. This ensures that the (discrete) variational formulation (13) has a unique solution, as a result of Theorem 1.2.

4.4 Finite Element Approximation

To discretize the variational problem defined in Section 4.2, suitable finite element spaces need to be constructed. The choice of finite element spaces has great impact on the accuracy and convergence of the method. In what follows we will assemble the conforming finite element space $\mathcal{W}_h \subset \mathcal{W}$ by constructing an approximation space for each individual subspace. The finite element space will therefore be built by five distinct finite element spaces, $\mathcal{W}_h = \mathcal{V}_h^\tau \times \mathcal{V}_h^v \times \mathcal{V}_h^n \times \mathcal{V}_h^\xi \times \mathcal{V}_h^q$, where the superscripts indicate the related quantity. As a consequence, we are looking for finite element spaces $\mathcal{V}_h^\tau \subset \bar{\boldsymbol{H}}_{\Gamma_D}(div;\Omega_S)$, $\mathcal{V}_h^v \subset \boldsymbol{H}^1(\Omega_S)$ and $\mathcal{V}_h^n \subset L^2(\Omega_S)$ in the structural domain Ω_S. For the fluid domain we need to define $\mathcal{V}_h^\xi \subset \bar{H}(div;\Omega_F)$ and $\mathcal{V}_h^q \subset H^1(\Omega_F)$.

Let $\mathcal{T}_h^S$ and $\mathcal{T}_h^F$ be regular, triangular partitions of the domains Ω_S and Ω_F, respectively. Let h denote the mesh size in both domains which we assume to be constant for all elements. For simplicity, we will assume the triangulations to be compatible along the interface Σ, meaning vertices of both meshes to overlap on the interface. We will furthermore denote edges by $(e_i)_i$ and vertices by $(x_i, y_i)_i$.

The finite element spaces $\mathcal{V}_h^v$ and $\mathcal{V}_h^q$ are constructed by continuous piecewise polynomials, as described in Section 3.1. For the velocity, each entry of the vector-valued space is constructed separately. The essential Dirichlet boundary conditions are easily imposed on the function space and we define

$$\mathcal{V}_{h,k}^v \coloneqq \{\boldsymbol{v}_h \in \mathcal{C}(\Omega_S) : \boldsymbol{v}_h|_T \in \boldsymbol{P}_k(T),\ \forall\ T \in \mathcal{T}_h^S \text{ and } \boldsymbol{v}_h|_{\Gamma_D} = 0\}\ .$$

Here we introduce $\boldsymbol{P}_k(T)$, the vector-valued polynomial functions up to degree k. For the fluid domain we define the finite element space for the pressure by

$$\mathcal{V}_{h,k}^q \coloneqq \{q_h \in \mathcal{C}(\Omega_F) : q_h|_T \in \mathcal{P}_k(T)\ \forall\ T \in \mathcal{T}_h^F\}\ .$$

It remains to fix the order of the of the approximations, k. Since it is desirable to obtain good approximations of the quantities as well as their first derivatives, an order of $k \geq 1$ will be necessary to capture both.

The vorticity can be discretized by piecewise polynomial functions, following Section 3.2,

$$\mathcal{V}_{h,k}^n \coloneqq \{\phi \in L^2(\Omega_S) : \phi|_T \in P_k(T)\ \forall T \in \mathcal{T}_h^S\}\ .$$

The error bound in Theorem 3.2 suggests $k \geq 0$ to be sufficient for convergence in h.

The stress in the structural domain and the pressure gradient in the fluid domain are discretized by Raviart-Thomas elements, as described in Section 3.3. The finite element space for the stress is constructed by combining two RT-elements. The essential Neumann boundary conditions can readily be incorporated into the function space,

$$\mathcal{V}_{h,k}^\tau \coloneqq \{\boldsymbol{\tau}|_T \in \bar{\boldsymbol{H}}(div;\Omega_S) \mid \boldsymbol{\tau} \in \boldsymbol{RT}_k(T)\ \forall\ T \in \mathcal{T}_h^S \text{ and } \boldsymbol{\tau\nu}|_{\Gamma_N} = 0\}\ .$$

Here, $\boldsymbol{RT}(T)$ is the tensor function space constructed by assembling two elements, $\phi_1,\ \phi_2$ of the vector function space $RT(T)$, $\boldsymbol{\tau} = \begin{bmatrix}\boldsymbol{\phi_1} & \boldsymbol{\phi_2}\end{bmatrix}^T$. The pressure gradient is approximated in the space

$$\boldsymbol{\mathcal{V}}_{h,k}^{\xi} \coloneqq \{\boldsymbol{\xi} \in \bar{H}(div;\Omega_F) \mid \boldsymbol{\xi} \in RT_k(T)\ \forall\ T \in \mathcal{T}_h^F\}\ .$$

To obtain accurate representations of the stress and pressure gradient we desire good approximations of the functions and its divergence. Following Theorem 3.4, choosing $k \geq 0$ is sufficient for convergence.

The finite element space for the fluid structure interaction is then constructed by

$$\mathcal{W}_{h,k} \coloneqq \mathcal{V}_{h,k}^{\tau} \times \mathcal{V}_{h,k+1}^{v} \times \mathcal{V}_{h,k}^{n} \times \mathcal{V}_{h,k}^{\xi} \times \mathcal{V}_{h,k+1}^{q}\ .$$

with order k. Note the increased order of $\mathcal{V}_{h,k+1}^{v}$ and $\mathcal{V}_{h,k+1}^{q}$ in this definition.

4.5 Discrete Variational Formulation

The finite element space gives rise to the discrete least-squares functional, $F_h : \mathcal{W}_{h,k} \to \mathbb{R}$,

$$\begin{aligned} F_h(\boldsymbol{\tau}_h, \boldsymbol{v}_h, n_h, \boldsymbol{\xi}_h, q_h; \boldsymbol{f}_S, f_F) = {} & \|\text{div}\ \boldsymbol{\tau_h} + \boldsymbol{f}_S\|_S^2 + \|\mathcal{C}^{-1}\boldsymbol{\tau}_h - \text{grad}\ \boldsymbol{v_h} + n_h\boldsymbol{\chi}\|_S^2 + \|sk(\boldsymbol{\tau}_h)\|_S^2 \\ & + \|\boldsymbol{\xi}_h - \text{grad}\ q_h\|_F^2 + \|\text{div}\ \boldsymbol{\xi_h} + f_F\|_F^2 \\ & + \|\boldsymbol{\tau}_h\boldsymbol{\nu}_F + q_h\boldsymbol{\nu}_F\|_\Sigma^2 + \|\boldsymbol{\xi}_h \cdot \boldsymbol{\nu}_F + \frac{\rho_F}{\rho_S}\boldsymbol{f}_S \cdot \boldsymbol{\nu}_F\|_\Sigma^2 \end{aligned} \tag{26}$$

and minimization problem

$$\arg \min_{(\boldsymbol{\tau}_h, \boldsymbol{v}_h, n_h, \boldsymbol{\xi}_h, q_h) \in \mathcal{W}_{h,k}} F_h(\boldsymbol{\tau}_h, \boldsymbol{v}_h, n_h, \boldsymbol{\xi}_h, q_h; \boldsymbol{f}_S, f_F) \tag{27}$$

over the finite dimensional space $\mathcal{W}_{h,k}$. The associated variational formulation reads: Find $(\boldsymbol{\sigma}_h, \boldsymbol{u}_h, m_h, \boldsymbol{\pi}_h, p_h) \in \mathcal{W}_{h,k}$ such that

$$\begin{aligned} & \langle \text{div}\ \boldsymbol{\sigma_h}, \text{div}\ \boldsymbol{\tau}\rangle_S + \langle \mathcal{C}^{-1}\boldsymbol{\sigma}_h, \mathcal{C}^{-1}\boldsymbol{\tau}\rangle_S + \langle sk(\boldsymbol{\sigma}_h), sk(\boldsymbol{\tau})\rangle_S \\ & - \langle \text{grad}\ \boldsymbol{u_h}, \mathcal{C}^{-1}\boldsymbol{\tau}\rangle_S - \langle \mathcal{C}^{-1}\boldsymbol{\sigma}_h, \text{grad}\ \boldsymbol{v}\rangle_S \\ & + \langle \text{grad}\ \boldsymbol{u_h}, \text{grad}\ \boldsymbol{v}\rangle_S \\ & - \langle \text{curl}\ \boldsymbol{u}_h, n\rangle_S - \langle \text{curl}\ \boldsymbol{v}, m\rangle_S \\ & + \langle m_h\boldsymbol{\chi}, \mathcal{C}^{-1}\boldsymbol{\tau}\rangle_S + \langle \mathcal{C}^{-1}\boldsymbol{\sigma}_h, n\boldsymbol{\chi}\rangle_S + 2m_h n \\ & + \langle \boldsymbol{\pi}_h, \boldsymbol{\xi}\rangle_F + \langle \text{div}\ \boldsymbol{\pi_h}, \text{div}\ \boldsymbol{\xi}\rangle_F \\ & - \langle \text{grad}\ p_h, \boldsymbol{\xi}\rangle_F - \langle \boldsymbol{\pi}_h, \text{grad}\ q\rangle_F \\ & + \langle \text{grad}\ p_h, \text{grad}\ q\rangle_F \\ & + \langle \boldsymbol{\sigma}_h\boldsymbol{\nu}_F, \boldsymbol{\tau}\boldsymbol{\nu}_F\rangle_\Sigma \\ & + \langle p_h\boldsymbol{\nu}_F, \boldsymbol{\tau}\boldsymbol{\nu}_F\rangle_\Sigma + \langle \boldsymbol{\sigma}_h\boldsymbol{\nu}_F, q\boldsymbol{\nu}_F\rangle_\Sigma \\ & + \langle \boldsymbol{\pi}_h \cdot \boldsymbol{\nu}_F, \boldsymbol{\xi} \cdot \boldsymbol{\nu}_F\rangle_\Sigma + \langle p_h\boldsymbol{\nu}_F, q\boldsymbol{\nu}_F\rangle_\Sigma \\ = {} & -\langle \boldsymbol{f}_S, \text{div}\ \boldsymbol{\tau}\rangle_S - \langle f_F, \text{div}\ \boldsymbol{\xi}\rangle_F + \langle \frac{\rho_F}{\rho_S}\boldsymbol{f}_S \cdot \boldsymbol{\nu}_F, \boldsymbol{\xi} \cdot \boldsymbol{\nu}_F\rangle_\Sigma \end{aligned} \tag{28}$$

for all $(\boldsymbol{\tau}, \boldsymbol{v}, n, \boldsymbol{\xi}, q) \in \mathcal{W}_h$. Existence and uniqueness for the discrete formulation is again given by Theorem 1.2 in conjunction with norm equivalence of the continuous least-squares

functional. The corresponding eigenvalueproblem then reads:
Find $\omega_h \in \mathbb{R}$, $(\boldsymbol{\sigma}_h, \boldsymbol{u}_h, m_h, \boldsymbol{\pi}_h, p_h) \in \mathcal{W}_{h,k}$ such that

$$\begin{aligned}
&\langle \text{div } \boldsymbol{\sigma_h}, \text{div } \boldsymbol{\tau}\rangle_S + \langle \mathcal{C}^{-1}\boldsymbol{\sigma}_h, \mathcal{C}^{-1}\boldsymbol{\tau}\rangle_S + \langle sk(\boldsymbol{\sigma}_h), sk(\boldsymbol{\tau})\rangle_S \\
&\quad - \langle \text{grad } \boldsymbol{u_h}, \mathcal{C}^{-1}\boldsymbol{\tau}\rangle_S - \langle \mathcal{C}^{-1}\boldsymbol{\sigma}_h, \text{grad } \boldsymbol{v}\rangle_S \\
&\quad + \langle \text{grad } \boldsymbol{u_h}, \text{grad } \boldsymbol{v}\rangle_S \\
&\quad - \langle \text{curl } \boldsymbol{u}_h, n\rangle_S - \langle \text{curl } \boldsymbol{v}, m\rangle_S \\
&\quad + \langle m_h\boldsymbol{\chi}, \mathcal{C}^{-1}\boldsymbol{\tau}\rangle_S + \langle \mathcal{C}^{-1}\boldsymbol{\sigma}_h, n\boldsymbol{\chi}\rangle_S + 2m_h n \\
&\quad + \langle \boldsymbol{\pi}_h, \boldsymbol{\xi}\rangle_F + \langle \text{div } \boldsymbol{\pi_h}, \text{div } \boldsymbol{\xi}\rangle_F \\
&\quad - \langle \text{grad } p_h, \boldsymbol{\xi}\rangle_F - \langle \boldsymbol{\pi}_h, \text{grad } q\rangle_F \\
&\quad + \langle \text{grad } p_h, \text{grad } q\rangle_F \\
&\quad + \langle \boldsymbol{\sigma}_h\boldsymbol{\nu}_F, \boldsymbol{\tau}\boldsymbol{\nu}_F\rangle_\Sigma \\
&\quad + \langle p_h\boldsymbol{\nu}_F, \boldsymbol{\tau}\boldsymbol{\nu}_F\rangle_\Sigma + \langle \boldsymbol{\sigma}_h\boldsymbol{\nu}_F, q\boldsymbol{\nu}_F\rangle_\Sigma \\
&\quad + \langle \boldsymbol{\pi}_h \cdot \boldsymbol{\nu}_F, \boldsymbol{\xi} \cdot \boldsymbol{\nu}_F\rangle_\Sigma + \langle p_h\boldsymbol{\nu}_F, q\boldsymbol{\nu}_F\rangle_\Sigma \\
&= (\omega_h)^2 \left(-\langle \rho_S \boldsymbol{u}, \text{div } \boldsymbol{\tau}\rangle_S - \langle \frac{1}{c^2} p, \text{div } \boldsymbol{\xi}\rangle_F + \langle \rho_F \boldsymbol{u} \cdot \boldsymbol{\nu}_F, \boldsymbol{\xi} \cdot \boldsymbol{\nu}_F\rangle_\Sigma \right)
\end{aligned} \tag{29}$$

4.6 Convergence Analysis and Error Estimates

In addition to existence and uniqueness to the minimization problem (27), Theorem 1.2 also ensures the quasioptimality of the least-squares solution:

Theorem 4.7 (Quasioptimality of the LS approximation)**.** *Let* $(\boldsymbol{\sigma}, \boldsymbol{u}, m, \boldsymbol{\pi}, p) \in \mathcal{W}$ *bet the solution of* (11) *and let* $(\boldsymbol{\sigma}_h, \boldsymbol{u}_h, m_h, \boldsymbol{\pi}_h, p_h) \in \mathcal{W}_{h,k}$ *be the solution of* (28)*. Then*

$$\begin{aligned}
&\|(\boldsymbol{\sigma} - \boldsymbol{\sigma}_h, \boldsymbol{u} - \boldsymbol{u}_h, m - m_h, \boldsymbol{\pi} - \boldsymbol{\pi}_h, p - p_h)\|_{\mathcal{W}} \\
&\quad \leq \alpha \inf_{(\boldsymbol{\tau}_h, \boldsymbol{v}_h, n_h, \boldsymbol{\xi}_h, q_h) \in \mathcal{W}_{h,k}} \|(\boldsymbol{\sigma} - \boldsymbol{\tau}_h, \boldsymbol{u} - \boldsymbol{v}_h, m - n_h, \boldsymbol{\pi} - \boldsymbol{\xi}_h, p - q_h)\|_{\mathcal{W}}
\end{aligned}$$

for some $\alpha > 0$*.*

An inherent a posteriori error estimate is given by the discrete LS functional. Moreover, the LS functional gives insight into the error distribution over the domain, creating the option to apply adaptive mesh refinement methods. To obtain an a priori error estimate we will first state the interpolation estimate for the space $\mathcal{W}_h$:

Theorem 4.8 (Approximation Property Finite Element Space)**.** *Let* $\Pi_h : \mathcal{W} \to \mathcal{W}_{h,k}$ *be the global interpolation operator described in the previous sections. Furthermore assume*

$$\begin{aligned}
&\boldsymbol{\sigma} \in \boldsymbol{H}^{k+1}(\Omega_S) \cap \bar{\boldsymbol{H}}_{\Gamma_N} \text{ and } div\, \boldsymbol{\tau} \in H^{k+1}(\Omega_S)\ , \\
&\boldsymbol{u} \in \boldsymbol{H}^{k+2}_{\Gamma_D}(\Omega_S)\ , \\
&m \in H^{k+1}(\Omega_S)\ , \\
&\boldsymbol{\pi} \in H^{k+1} \cap \bar{H}(div; \Omega_F)\ , \\
&p \in H^{k+2}(\Omega_F)\ .
\end{aligned}$$

Then we obtain the interpolation estimate

$$\|(\boldsymbol{\sigma}, \boldsymbol{u}, m, \boldsymbol{\pi}, p) - \Pi_h(\boldsymbol{\sigma}, \boldsymbol{u}, m, \boldsymbol{\pi}, p)\|_{\mathcal{W}} \leq \alpha h^{k+1} \|(\boldsymbol{\sigma}, \boldsymbol{u}, m, \boldsymbol{\pi}, p)\|_{\mathcal{W}}\ .$$

Proof. The theorem follows from the approximation estimates presented in Theorem 3.1, Theorem 3.4 and Theorem 3.2. □

We can now formulate an a priori error esimator:

Theorem 4.9 (A priori error estimate)**.** *Let* $(\boldsymbol{\sigma}, \boldsymbol{u}, m, \boldsymbol{\pi}, p) \in \mathcal{W}$ *be the exact solution to the system* (11)*. Let* $(\boldsymbol{\sigma}_h, \boldsymbol{u}_h, m_h, \boldsymbol{\pi}_h, p_h) \in \mathcal{W}_{h,k}$ *be the solution to* (28)*. Furthermore assume*

$$\begin{aligned}
&\boldsymbol{\sigma} \in \boldsymbol{H}^{k+1}(\Omega_S) \cap \bar{\boldsymbol{H}}_{\Gamma_N} \text{ and } div\, \boldsymbol{\tau} \in H^{k+1}(\Omega_S) \ , \\
&\boldsymbol{u} \in \boldsymbol{H}^{k+2}_{\Gamma_D}(\Omega_S) \ , \\
&m \in H^{k+1}(\Omega_S) \ , \\
&\boldsymbol{\pi} \in H^{k+1} \cap \bar{H}(div; \Omega_F) \ , \\
&p \in H^{k+2}(\Omega_F) \ .
\end{aligned}$$

Then

$$F(\boldsymbol{\sigma}_h, \boldsymbol{u}_h, m_h, \boldsymbol{\pi}_h, p_h; \boldsymbol{f}_S, f_F) \leq \alpha h^{k+1} \|(\boldsymbol{\sigma}, \boldsymbol{u}, m, \boldsymbol{\pi}, p)\|_{\mathcal{W}}$$

for some $\alpha > 0$ *and given* $\boldsymbol{f}_S \in \boldsymbol{H}^1(\Omega_S)$, $f_F \in L^2(\Omega_F)$.

Proof. Using the continuity of the LS functional, Theorem 4.6,

$$\begin{aligned}
F(\boldsymbol{\sigma}_h, \boldsymbol{u}_h, m_h, \boldsymbol{\pi}_h, p_h; \boldsymbol{f}_S, f_F) &= F(\boldsymbol{\sigma} - \boldsymbol{\sigma}_h, \boldsymbol{u} - \boldsymbol{u}_h, m - m_h, \boldsymbol{\pi} - \boldsymbol{\pi}_h, p - p_h; \boldsymbol{0}, 0) \\
&\leq \alpha \|(\boldsymbol{\sigma} - \boldsymbol{\sigma}_h, \boldsymbol{u} - \boldsymbol{u}_h, m - m_h, \boldsymbol{\pi} - \boldsymbol{\pi}_h, p - p_h)\|_{\mathcal{W}} \\
&\leq \alpha h^{k+1} \|(\boldsymbol{\sigma}, \boldsymbol{u}, m, \boldsymbol{\pi}, p)\|_{\mathcal{W}} \ .
\end{aligned}$$

In the last step we used $\Pi_h(\boldsymbol{\sigma}, \boldsymbol{u}, m, \boldsymbol{\pi}, p) = (\boldsymbol{\sigma}_h, \boldsymbol{u}_h, m_h, \boldsymbol{\pi}_h, p_h)$ and applied the interpolation estimate of Theorem 4.8. □

Besides an a priori estimator, Theorem 4.9 ensures convergences for sufficiently smooth exact solutions.

5 Numerical Implementations

We will formulate the matrix equations of the fluid-structure interaction in Section 5.1 followed by some notes on the implementation. In Section 5.2 we state the numerical results for the implementation.

5.1 Matrix Formulation

Rewriting the discrete variational formulation (29) to a matrix equation requires the evaluation of inner products of basis functions. By doing so, we obtain a system of the the form

$$\begin{bmatrix} A_\sigma & A_{\sigma,u} & A_{\sigma,m} & \mathbf{0} & C_{\sigma,p} \\ A_{\sigma,u}^T & A_u & A_{u,m} & \mathbf{0} & \mathbf{0} \\ A_{\sigma,m}^T & A_{u,m}^T & A_m & \mathbf{0} & \mathbf{0} \\ \mathbf{0} & \mathbf{0} & \mathbf{0} & B_\pi & B_{\pi,p} \\ C_{\sigma,p}^T & \mathbf{0} & \mathbf{0} & B_{\pi,p}^T & B_p \end{bmatrix} \begin{bmatrix} \vec{\sigma} \\ \vec{u} \\ \vec{m} \\ \vec{\pi} \\ \vec{p} \end{bmatrix} = (\omega_h)^2 \begin{bmatrix} \mathbf{0} & \mathbf{0} & \mathbf{0} & \mathbf{0} & \mathbf{0} \\ -\rho_S F_{\sigma,\sigma}^T & \mathbf{0} & \mathbf{0} & \mathbf{0} & \mathbf{0} \\ \mathbf{0} & \mathbf{0} & \mathbf{0} & \mathbf{0} & \mathbf{0} \\ \mathbf{0} & \rho_F E_{u,\xi}^T & \mathbf{0} & \mathbf{0} & -\frac{1}{c^2} F_{\pi,p} \\ \mathbf{0} & \mathbf{0} & \mathbf{0} & \mathbf{0} & \mathbf{0} \end{bmatrix} \begin{bmatrix} \vec{\sigma} \\ \vec{u} \\ \vec{m} \\ \vec{\pi} \\ \vec{p} \end{bmatrix}$$

where on the left-hand side A indicates operators associated with the solid domain, B indicates operators associated with the fluid domain and C indicates operators associated with the interface. The subscripts refer to the related quantities, for example $A_{\sigma,u}$ is associated with the bilinear form $-\langle \operatorname{grad} \boldsymbol{u}, \mathcal{C}^{-1}\boldsymbol{\tau}\rangle_S$ and $A_{\sigma,u}^T$ with $-\langle \mathcal{C}^{-1}\boldsymbol{\sigma}, \operatorname{grad} \boldsymbol{v}\rangle_S$. On the right-hand side we denote by $F_{\sigma,u}$ the operator associated with $\langle \boldsymbol{u}, \operatorname{div} \boldsymbol{\tau}\rangle_S$, $F_{\pi,p}$ with $\langle p, \operatorname{div} \boldsymbol{\xi}\rangle_F$ and $F_{u,\xi}$ with $\langle \boldsymbol{u}\cdot\boldsymbol{\nu}_F, \boldsymbol{\xi}\cdot\boldsymbol{\nu}_F\rangle_\Sigma$.

The matrix on the left-hand side is symmetric and positive-definite. This is ensured by the Rayleigh-Ritz-like setting of Theorem 1.2. Clearly, symmetry of the right-hand side is not given. It is useful to rewrite the system to obtain symmetric matrices at both sides. One way to achieve this is to rewrite the system to an equivalent symmetric formulation, as is done in [4] or [1]. However, in our case, this step is not as straightforward and we have therefore decided to leave the system in its original form. This choice has the disadvantage that we cannot draw any conclusions about whether the system has real eigenvalues.
For the implementations of the problem we construct two separate finite element systems, one for the fluid domain and one for the solid domain. For simplicity, we rewrite the system to

$$\begin{bmatrix} \boldsymbol{A}_S & \boldsymbol{C} \\ \boldsymbol{C}^T & \boldsymbol{A}_F \end{bmatrix} \begin{bmatrix} \vec{x}_S \\ \vec{x}_F \end{bmatrix} = (\omega_h)^2 \begin{bmatrix} \boldsymbol{F}_S & \mathbf{0} \\ \boldsymbol{E} & \boldsymbol{F}_F \end{bmatrix} \begin{bmatrix} \vec{x}_S \\ \vec{x}_F \end{bmatrix}$$

where the matrices for the solid, fluid and structural part are combined. To be able to apply standard eigenvalue solvers we rewrite the system to

$$\frac{1}{(\omega_h)^2} \begin{bmatrix} \boldsymbol{A}_S & \boldsymbol{C} \\ \boldsymbol{C}^T & \boldsymbol{A}_F \end{bmatrix} \begin{bmatrix} \vec{x}_S \\ \vec{x}_F \end{bmatrix} = \begin{bmatrix} \boldsymbol{F}_S & \mathbf{0} \\ \boldsymbol{E} & \boldsymbol{F}_F \end{bmatrix} \begin{bmatrix} \vec{x}_S \\ \vec{x}_F \end{bmatrix}$$

and solve for $\frac{1}{(\omega_h)^2}$. The computation of the matrices $\boldsymbol{A}_S$, $\boldsymbol{A}_F$, $\boldsymbol{F}_S$ and $\boldsymbol{F}_F$ are is done in the usual manner, and is carried out using the build-in functions of *FEniCS*. Computing the coupling matrices $\boldsymbol{C}$ and $\boldsymbol{E}$ is, to the knowledge of the author, not directly possible in *FEniCS* and will therefore be calculated manually. We now proceed with the definitions of C and E. To keep calculations as simple as possible, we consider the lowest order finite element space $\mathcal{W}_{h,0}$. Note that the order of Raviart-Thomas functions is defined differently in *FEniCS* and that the lowest order corresponds to the definitions provided

below. Furthermore, Raviart-Thomas tensor and vector elements are constructed using *VectorElement* and *FintieElement*, respectively. In total, we employ the following spaces in *FEniCS*:

$\sigma \in$ `VectorElement('RT', 1)`
$u \in$ `VectorElement('CG', 1)`
$m \in$ `FiniteElement('DG', 0)`
$\pi \in$ `FiniteElement('RT', 1)`
$p \in$ `FiniteElement('CG', 1)`

We start by manually obtaining the operators for $\langle p_h \boldsymbol{\nu}_F, \boldsymbol{\tau}\boldsymbol{\nu}_F \rangle_\Sigma$ and $\langle \boldsymbol{\sigma}_h \boldsymbol{\nu}_F, q\boldsymbol{\nu}_F \rangle_\Sigma$ for the lowest-order Raviart-Thomas elements and first-order Lagrangian elements. The procedure is as follows:

Let e_i denote the edges associated with the solid mesh and $\boldsymbol{\psi}_i$, $0 \leq i \leq N$ the corresponding Raviart-Thomas basis function. One can readily show that $\boldsymbol{\psi}_i \cdot \boldsymbol{\nu}_S|_{e_j} = \delta_{i,j}$ is constant along the edge e_j. The basis functions for the Raviart-Thomas tensor space are now constructed using $\boldsymbol{\tau}_{lk} = \begin{bmatrix} \boldsymbol{\phi}_l^T \\ \boldsymbol{\phi}_k^T \end{bmatrix}$, with $(\boldsymbol{\phi}_l)_{l \geq 0}$ the basis function for the Raviart-Thomas vector space.
We denote the Lagrangian basis functions by ψ_i, $0 \leq i \leq N$ and compute

$$\begin{aligned}
\langle p_h \boldsymbol{\nu}_F, \boldsymbol{\tau}_{lk} \boldsymbol{\nu}_F \rangle_\Sigma &= \langle p_h \boldsymbol{\nu}_F, \begin{bmatrix} \boldsymbol{\phi}_l^T \\ \mathbf{0} \end{bmatrix} \boldsymbol{\nu}_F \rangle_{e_l} + \langle p_h \boldsymbol{\nu}_F, \begin{bmatrix} \mathbf{0} \\ \boldsymbol{\phi}_k^T \end{bmatrix} \boldsymbol{\nu}_F \rangle_{e_k} \\
&= \langle \left(\sum_{i=0}^{N} p_i \psi_i \right) \boldsymbol{\nu}_F, \begin{bmatrix} -1 \\ 0 \end{bmatrix} \rangle_{e_l} + \langle \left(\sum_{i=0}^{N} p_i \psi_i \right) \boldsymbol{\nu}_F, \begin{bmatrix} 0 \\ -1 \end{bmatrix} \rangle_{e_k} \\
&= -\nu_{F,x} \frac{|e_l|}{2} p_{l-1} - \nu_{F,x} \frac{|e_l|}{2} p_l - \nu_{F,y} \frac{|e_k|}{2} p_{k-1} - \nu_{F,y} \frac{|e_k|}{2} p_k \\
&= \begin{bmatrix} -\nu_{F,x} \frac{|e_l|}{2} & -\nu_{F,x} \frac{|e_l|}{2} & -\nu_{F,y} \frac{|e_k|}{2} & -\nu_{F,y} \frac{|e_k|}{2} \end{bmatrix} \begin{bmatrix} p_{l-1} \\ p_l \\ p_{k-1} \\ p_k \end{bmatrix},
\end{aligned} \tag{30}$$

where $\nu_{F,x}$ and $\nu_{F,y}$ denote the first and second component of the normal vector. Similarly, for a Lagrangian basis function q_i with nonzero value on e_i and e_{i-1}:

$$\begin{aligned}
\langle \boldsymbol{\sigma}_h \boldsymbol{\nu}_F, q_i \boldsymbol{\nu}_F \rangle_\Sigma &= \langle \boldsymbol{\sigma}_h \boldsymbol{\nu}_F, q_i \boldsymbol{\nu}_F \rangle_{e_{i-1}} + \langle \boldsymbol{\sigma}_h \boldsymbol{\nu}_F, q_i \boldsymbol{\nu}_F \rangle_{e_i} \\
&= \langle \begin{bmatrix} \sigma_{i-1}^1 \boldsymbol{\phi}_{i-1}^T \\ \sigma_{i-1}^2 \boldsymbol{\phi}_{i-1}^T \end{bmatrix} \boldsymbol{\nu}_F, q_i \boldsymbol{\nu}_F \rangle_{e_{i-1}} + \langle \begin{bmatrix} \sigma_i^1 \boldsymbol{\phi}_i^T \\ \sigma_i^2 \boldsymbol{\phi}_i^T \end{bmatrix} \boldsymbol{\nu}_F, q_i \boldsymbol{\nu}_F \rangle_{e_i} \\
&= \langle \begin{bmatrix} -\sigma_{i-1}^1 \\ -\sigma_{i-1}^2 \end{bmatrix}, q_i \boldsymbol{\nu}_F \rangle_{e_{i-1}} + \langle \begin{bmatrix} -\sigma_i^1 \\ -\sigma_i^2 \end{bmatrix}, q_i \boldsymbol{\nu}_F \rangle_{e_i} \\
&= -\frac{|e_{i-1}|}{2} \nu_{F,x} \sigma_{i-1}^1 - \frac{|e_{i-1}|}{2} \nu_{F,y} \sigma_{i-1}^2 - \frac{|e_i|}{2} \nu_{F,x} \sigma_i^1 - \frac{|e_i|}{2} \nu_{F,y} \sigma_i^1 \\
&= \begin{bmatrix} -\frac{|e_{i-1}|}{2} \nu_{F,x} & -\frac{|e_{i-1}|}{2} \nu_{F,y} & -\frac{|e_i|}{2} \nu_{F,x} & -\frac{|e_i|}{2} \nu_{F,y} \end{bmatrix} \begin{bmatrix} \sigma_{i-1}^1 \\ \sigma_{i-1}^2 \\ \sigma_i^1 \\ \sigma_i^2. \end{bmatrix}
\end{aligned} \tag{31}$$

Equations (30) and (31) define the rows of the matrices C and C^T. It is easy to see that the constructed matrices are indeed transposes of each other.

For the matrix on the right-hand side let $\boldsymbol{\xi}_i$ denote the lowest order Raviart-Thomas element. Then,

$$\begin{aligned}\langle \boldsymbol{u}_h \cdot \boldsymbol{\nu}_F, \boldsymbol{\xi}_i \cdot \boldsymbol{\nu}_F \rangle_\Sigma &= \langle \boldsymbol{u}_h \cdot \boldsymbol{\nu}_F, \boldsymbol{\xi}_i \cdot \boldsymbol{\nu}_F \rangle_{e_i} = \langle \boldsymbol{u}_h \cdot \boldsymbol{\nu}_F, 1 \rangle_{e_i} \\ &= \begin{bmatrix} \frac{|e_i|}{2}\nu_{F,x} & \frac{|e_i|}{2}\nu_{F,y} & \frac{|e_i|}{2}\nu_{F,x} & \frac{|e_i|}{2}\nu_{F,y} \end{bmatrix} \begin{bmatrix} u_{i-1}^1 \\ u_{i-1}^2 \\ u_i^1 \\ u_i^2 \end{bmatrix}\end{aligned}$$

for $\boldsymbol{u}_h$ approximated by first order Lagrangian vector elements. This forms the entries of the matrix $\boldsymbol{E}$ and concludes drawing up the discrete system.

5.2 Numerical Results

For the numerical experiment we consider a two-dimensional steel container filled with water, more precisely, we use the same setup as introduced by Bermudez et al. in [1]. Typical quantities are, see for example [1] or [19],

- $\nu_P = 0.35$,
- $E = 1.4410^{11}$ Pa ,
- $\rho_S = 7700$ Kg/m ^{3} ,
- $\rho_F = 1000$ Kg/m ^{3} ,
- $c = 1430$ m/s .

The elasticity modulus E and Poisson ratio ν_P give rise to the Lamé coefficients by

$$\lambda = \frac{E\nu_P}{(1+\nu_P)(1-2\nu_P)} \quad \text{and} \quad \mu = \frac{E}{2(1+\nu_P)} \ .$$

The fluid domain will cover the unit square, the solid domain encloses the fluid domain, as shown in Figure 8. The structure is fixed at the bottom and is free of stress at all other boundaries. A regular triangular mesh is constructed for the domains, as shown in Figure 9. Both meshes are constructed such that the vertices on the interface coincide and the mesh diameter of both meshes coincides. We furthermore define the refinement parameter N to be linear to the number of element layers across the thickness of the solid. An example of the mesh is shown in Figure 9, where $N = 2$ is adopted. Note that the diameter h of the mesh is halved if the refinement parameter is doubled. The number of cells for both meshes as well as the number of d.o.f. of each formulation are listed in Table 1. The eigenvalue problem is constructed as described in Section 5.1. The computed eigenfrequencies $(\omega_h)_i$ for the first three modes are listed in Table 2. Several eigenfunctions are shown in Figure 10. Here, we plotted the first eigenfunction for meshes with $N = 4$ and $N = 8$ to compare the same eigenfunctions on different meshes. Furthermore, the third eigenfunction for $N = 4$ is depicted. Here, the obtained eigenvalue is close the reference case by Bermudez et al. described in the next section, and comparison of the eigenfunctions is of interest.

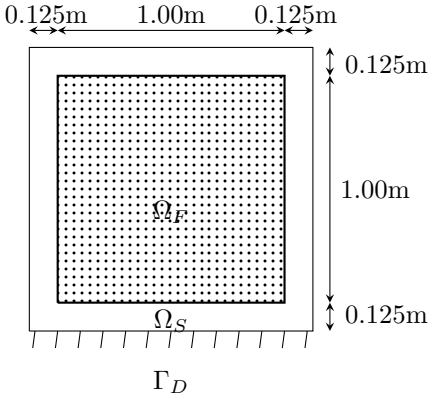

Figure 8: Steel cavity with water inside.

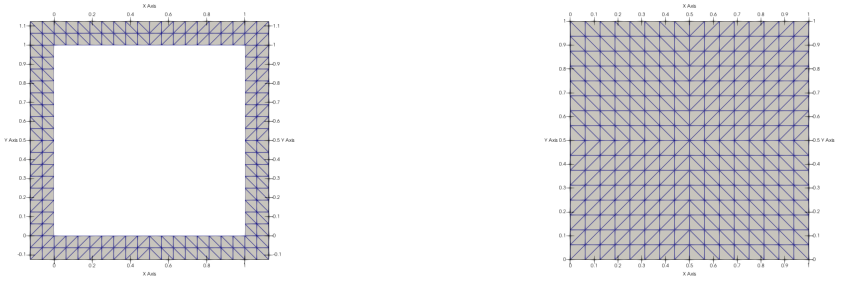

Figure 9: Meshes for the solid domain (left) and the fluid domain (right) for $N = 2$.

Table 1: Number of cells and d.o.f. in each subdomain.

N	cells Ω_S	cells Ω_F	d.o.f. Ω_S	d.o.f. Ω_F
2	288	512	1728	1089
4	1152	2048	6336	4225
8	4068	8192	24192	16641
16	19584	32768	94464	66049

Table 2: First eigenfrequencies in [rad/s].

Mode	$N = 2$	$N = 4$	$N = 8$	$N = 16$
1st	214.4287	$69.8921 \pm 48.5747j$	79.3296	68.4049 ± 10.5005
2nd	$340.2275 \pm 148.8240j$	$129.2544 \pm 47.4294j$	137.9913	70.2523
3rd	349.5590	279.5397	$174.5258 + 61.9401j$	70.3725

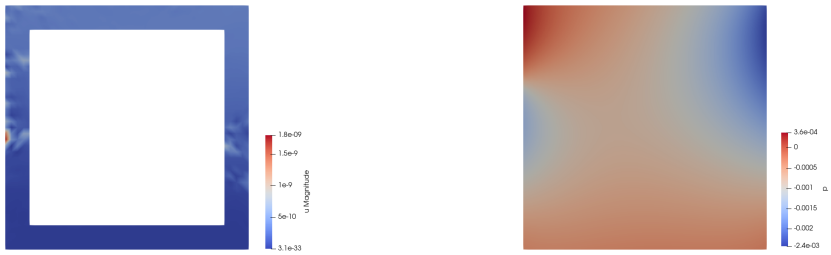

(a) Eigensolutions corresponding with ω_1 for $N = 4$

(b) Eigensolutions corresponding with ω_1 for $N = 8$.

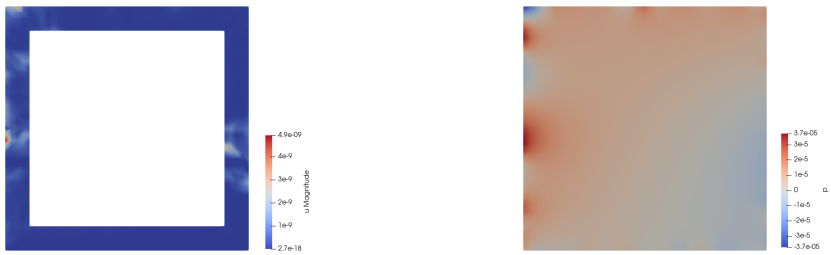

(c) Eigensolutions corresponding with ω_3 for $N = 4$.

Figure 10: Examples of eigenfunctions at several levels of refinement.

The lack of convergence of the results in Table 2 suggests that the developed method does not produce meaningful results at this stage. Comparing these results to the results presented in [1], we observe that the real parts of the eigenvalues obtained here are within the same range as [1] for some specific settings. Despite this, there is no complete agreement. In addition, the eigenvalues do not converge when refining the mesh. This could have various reasons. Firstly, we constructed the least-squares functional using solely L^2-norms. As already mentioned in Section 4, replacing the trace-norms in the LS functional yields suboptimal results. In [23], Stevenson elaborates on the effects and suggests preconditioning of the LS functional whenever replacing norms. Secondly, taking a closer look at the conditioning of the eigenvalueproblem shows some cause for computational issues. In particular, the Lamé coefficients are of order $\mu \approx 10^{10}$ and $\lambda \approx 10^{11}$. The inner products use the evaluation of $\left(\frac{\lambda}{2\mu(2\mu+2\lambda)}\right)^2$. This fact, in combination with aiming for a small eigenvalue of the form $\frac{1}{(\omega_h)^2}$, is expected to yield inaccurate results. Comparing the eigenfunctions depicted in Figure 10 with the expected results presented in the next section also implies faulty results. Not only is the solution for refined meshes not consistent, physical interpretation is also not evident.

To verify whether convergence improves when different values of μ and λ are chosen we run additional simulations with the made-up constants

- $\lambda = 100$ Pa,
- $\mu = 10$ Pa.

The remaining constants are unchanged. The results can be found in Table 3.

Table 3: First eigenfrequencies in [rad/s] with $\lambda = 100$ and $\mu = 10$.

Mode	$N = 2$	$N = 4$	$N = 8$	$N = 16$
1st	965.4107	986.8243	981.0819	981.1344
2nd	988.5367	984.3537	984.5058	984.3174
3rd	1016.6279	1012.3534	1011.4935	1011.5444
4th	1595.9532	1258.5902	1251.9838	1251.9068
5th	1770.5451	1551.0105	1548.3767	1560.2639

Although the method shows convergence the computed order of convergence on each step does not give a precise indication yet. The obtained orders of convergence are given in Table 4. The first eigenmodes for the structural displacement and the fluid pressure are shown in Figure 11. The eigenfunction of the fluid pressure describe a plausible eigenmode. For the structural displacement, a physical interpretation is not as apparent, as we would expect the largest displacements along the Neumann boundary. While the convergence of the eigenvalues provides confidence in the obtained numerical results for this made-up setting, verification by comparison with literature is unfortunately not possible.

Table 4: Convergence order with $\lambda = 100$ and $\mu = 10$.

Mode	order α_4	order α_8
1st	1.899	6.772
2nd	4.781	−0.309
3rd	2.314	4.0782
4th	5.674	6.423
5th	6.381	−2.174

Figure 11: Structural displacement (left) and fluid pressure (right) for ω_1, $\lambda = 100$, $\mu = 10$ and $N = 16$.

6 Least-Squares Functional as Error Estimator

Additionally to deriving a finite element formulation, the LS functional can also be exploited as an error estimate for otherwise derived discrete models. In this section, we first present the pressure/displacement formulations for the fluid structure interaction. Subsequently, we apply the LS functional as error estimator and present numerical results.

6.1 The Pressure-Displacement Formulation

To avoid the inaccurate results obtained by the LS formulation described in the previous section, we resort to the pressure-displacement formulation of the fluid-structure interaction problem presented by Bermudez et al. in [1]. Here, the primal formulation of the problem is kept,

$$\begin{aligned}
&\operatorname{div}\, \sigma(u) + \omega^2 \rho_S \boldsymbol{u} = \boldsymbol{0} && \text{in } \Omega_S \ , \\
&\Delta p + \frac{\omega^2}{c^2} p = 0 && \text{in } \Omega_F \ , \\
&\boldsymbol{u} = \boldsymbol{0} && \text{on } \Gamma_D \ , \\
&\sigma(\boldsymbol{u}) = \boldsymbol{0} && \text{on } \Gamma_N \ , \\
&\sigma(\boldsymbol{u})\boldsymbol{\nu}_F + p\boldsymbol{\nu}_F = \boldsymbol{0} && \text{on } \Sigma \ , \\
&\frac{1}{\rho_F}\frac{\partial p}{\partial \boldsymbol{\nu}_F} - \omega^2 \boldsymbol{u}\cdot\boldsymbol{\nu}_F = 0 && \text{on } \Sigma \ .
\end{aligned}$$

Note that σ adopted here is not the same as $\boldsymbol{\sigma}$ used in previous sections. Instead, σ is the function describing

$$\sigma(\boldsymbol{u}) = \mathcal{C}(\epsilon(\boldsymbol{u})) \ ,$$

describing Hooke's Law. The weak form reads: Find $\omega \in \mathbb{R}$ and $\boldsymbol{0} \neq (\boldsymbol{u}, p) \in \mathcal{V}$ such that

$$\begin{aligned}
&\langle \sigma(\boldsymbol{u}), \boldsymbol{\epsilon}(\boldsymbol{u}) \rangle_S + \langle \frac{1}{\rho_F} \nabla p, \nabla q \rangle_F - \langle p, \boldsymbol{v}\cdot\boldsymbol{\nu}_F \rangle_\Sigma \\
&\quad = \omega^2 \langle \rho_S \boldsymbol{u}, \boldsymbol{v} \rangle_S + \omega^2 \langle \frac{1}{\rho_F c^2} p, q \rangle_F + \omega^2 \langle \boldsymbol{u}\cdot\boldsymbol{\nu}_F, q \rangle_\Sigma \ \forall (\boldsymbol{v}, q) \in \mathcal{V} \ ,
\end{aligned}$$

for $\mathcal{V} \coloneqq \boldsymbol{H}^1_{\Gamma_D}(\Omega_S) \times H^1(\Omega_F)$. Approximating the solution space with appropriate finite element spaces leads to the matrix formulation

$$\begin{bmatrix} \boldsymbol{K}^S & -\boldsymbol{C} \\ \boldsymbol{0} & \frac{1}{\rho_F}\boldsymbol{K}^F_P \end{bmatrix} \begin{bmatrix} \boldsymbol{U}^S \\ \boldsymbol{P} \end{bmatrix} = (\omega_h)^2 \begin{bmatrix} \boldsymbol{M}^S & \boldsymbol{0} \\ \boldsymbol{C}^T & \frac{1}{\rho_F c^2}\boldsymbol{M}^F_P \end{bmatrix} \begin{bmatrix} \boldsymbol{U}^S \\ \boldsymbol{P} \end{bmatrix} \ .$$

This problem is ill-conditioned, prompting Bermudez et al. to solve

$$\begin{bmatrix} \boldsymbol{K}^S & -\boldsymbol{C} \\ \boldsymbol{0} & \delta\frac{1}{\rho_F}\boldsymbol{K}^F_P \end{bmatrix} \begin{bmatrix} \boldsymbol{U}^S \\ \boldsymbol{P} \end{bmatrix} = \eta^2 \begin{bmatrix} \boldsymbol{M}^S - \delta\boldsymbol{K}^S & \delta\boldsymbol{C} \\ \delta\boldsymbol{C}^T & \delta\left(\frac{1}{\rho_F c^2}\boldsymbol{M}^F_P - \delta\boldsymbol{K}^F_P\right) \end{bmatrix} \begin{bmatrix} \boldsymbol{U}^S \\ \boldsymbol{P} \end{bmatrix}$$

with $\eta^2 = (\omega_h)^2/[1 - \delta(\omega_h)^2]$. This reformulation assures a symmetric positive definite right hand side, provided that $\delta > 0$ is sufficiently small. For a more detailed derivation we refer to the paper by Bermudez et al..

6.2 Numerical Results: Pressure-Displacement Formulation

Numerical validation is carried out using the same setup as described in Section 5.2. The finite element spaces for the displacement $\boldsymbol{u}$ and pressure p, $\mathcal{V}_h = \mathcal{V}_{h,1}^v \times \mathcal{V}_{h,1}^1$ are chosen as the spaces of first-order piecewise polynomial functions, identical to the LS setting previously presented. With meshes as in Section 5.2, we note the degrees of freedom for both subdomains in Table 5. It is worth mentioning that the number of d.o.f. in this setting is significantly smaller than used in Section 5.2. This is a direct result of the absence of various variables in the approach used in this section.

Table 5: Number of cells and d.o.f. in each subdomain for the pressure/displacement formulation.

N	cells Ω_S	cells Ω_F	d.o.f. Ω_S	d.o.f. Ω_F
2	288	512	432	289
4	1152	2048	1440	1089
8	4068	8192	5184	4225
16	18432	32768	19584	16641

Table 6: Eigenfrequencies for the pressure/displacement formulation in [rad/s].

Mode	$N = 2$	$N = 4$	$N = 8$	$N = 16$
1st	87.9299	66.9007	63.7641	63.2626
2nd	299.9612	237.3229	227.1345	225.3493
3rd	480.5712	384.5606	367.7761	364.9972

The given experiment yields the eigenfrequencies presented in Table 6. These frequencies coincide with the results found by Bermudez et al.. The corresponding eigenfunctions for the first three eigenmodes for the mesh with refinement parameter $N = 4$ are depicted in Figure 12. The measured order of convergence of the eigenvalues is $\frac{5}{2}$, as given in Table 7.

Table 7: Order of convergence of the eigenvalues with the pressure/displacement formulation.

Mode	order α_4	order α_8
1st	2.74512	2.64488
2nd	2.62012	2.51277
3rd	2.51606	2.59454

(a) Displacement and pressure for $\omega_{h,1}$.

(b) Displacement and pressure for $\omega_{h,2}$.

(c) Displacement and pressure for $\omega_{h,3}$.

Figure 12: First three eigenfunctions obtained at N=4. For each eigenfunction, the displacement (left) and pressure (right) are shown.

6.3 Least-Squares Functional as Error Estimator

To utilize the LS functional as an error estimate one first has to compute the missing quantities, $\boldsymbol{\sigma}$, m and π. These quantities are obtained by projecting the variables to finite element spaces used in the LS setting. These spaces are $\mathcal{V}_{h,0}^{\tau}$, $\mathcal{V}_{h,0}^{n}$ and $\mathcal{V}_{h,0}^{\xi}$, respectively. Using

$$\begin{aligned}\boldsymbol{\sigma} &= \mathcal{C}^{-1}\epsilon(\boldsymbol{u}) \ ,\\ m &= \frac{1}{2}\nabla \times \boldsymbol{u} \ ,\\ \boldsymbol{\pi} &= \text{grad } p \ ,\end{aligned}$$

the variables are obtained by solving

$$\begin{aligned}\langle \mathcal{C}\boldsymbol{\sigma}, \boldsymbol{\tau}\rangle_S &= \langle \epsilon(\boldsymbol{u}), \boldsymbol{\tau}\rangle_S \quad \forall \boldsymbol{\tau} \in \mathcal{V}_{h,0}^{\tau} \ ,\\ \langle m, n\rangle_S &= \langle \frac{1}{2}\nabla \times \boldsymbol{u}, n\rangle_S \quad \forall n \in \mathcal{V}_{h,0}^{n} \ ,\\ \langle \pi, \xi\rangle_F &= \langle \text{grad } p, \xi\rangle_F \quad \forall \xi \in \mathcal{V}_{h,0}^{\xi} \ .\end{aligned}$$

The LS functional can now readily be evaluated over both subdomains. The terms defined over the interface are assembled manually, similarly as is done in Section 5.1. To gain more insight into the behavior of the LS functional, we split the function into its separate subfunctionals

$$F(\boldsymbol{\tau}, \boldsymbol{\xi}, n, \boldsymbol{\xi}, q) = F_{S1}(\boldsymbol{\tau}, \boldsymbol{v}) + F_{S2}(\boldsymbol{\tau}, \boldsymbol{v}, n) + F_{S3}(\boldsymbol{\tau}) + F_{F1}(\boldsymbol{\xi}, q) + F_{F2}(\boldsymbol{\xi}, q) + F_{\Sigma 1}(\boldsymbol{\tau}, q) + F_{\Sigma 2}(\xi)$$

with

$$\begin{aligned}F_{S1}(\boldsymbol{\tau}, \boldsymbol{v}) &= \|\text{div } \boldsymbol{\tau} + \omega^2 \rho_S \boldsymbol{u}\|_S^2 \ ,\\ F_{S2}(\boldsymbol{\tau}, \boldsymbol{v}, n) &= \|\mathcal{C}^{-1}\boldsymbol{\tau} - \text{grad } \boldsymbol{v} + n\boldsymbol{\chi}\|_S^2 \ ,\\ F_{S3}(\boldsymbol{\tau}) &= \|sk(\boldsymbol{\tau})\|_S^2 \ ,\\ F_{F1}(\boldsymbol{\xi}, q) &= \|\boldsymbol{\xi} - \text{grad } q\|_F^2 \ ,\\ F_{F2}(\boldsymbol{\xi}, q) &= \|\text{div } \boldsymbol{\xi} + \frac{\omega^2}{c^2} p\|_F^2 \ ,\\ F_{\Sigma 1}(\boldsymbol{\tau}, q) &= \|\boldsymbol{\tau}\boldsymbol{\nu}_F + q\boldsymbol{\nu}_F\|_{\Sigma}^2 \ ,\\ F_{\Sigma 2}(\xi) &= \|\boldsymbol{\xi} \cdot \boldsymbol{\nu}_F - \omega^2 \rho_F \boldsymbol{u} \cdot \boldsymbol{\nu}_F\|_{\Sigma}^2 \ .\end{aligned}$$

For the first eigenvalue, the errors for each subterm are listed in Table 8. Firstly, we see that F_{S3} is consistently zero. This is a result of the construction of $\boldsymbol{\sigma}$ and follows directly from the symmetry of $\epsilon(\boldsymbol{u})$. For this reason we omit F_{S3} from further discussion. All other terms, except for F_{S1}, are converging towards zero with mesh refinement. The reason why the first term is not converging is not entirely clear, one can however note that the error of the F_{S1} is relatively large. This could again be due to the physical coefficients λ, μ and $\omega^2\rho_S$ being of order 10^{10}. Although the errors of the interface functionals seem to converge, the errors are relatively large. Here, too, we observe that these errors contain terms that depend on μ, λ, and $\omega^2\rho_F$.

The order of convergence for some subfunctionals are listed in Table 9. For F_{S2} and F_{F1} the order is at least one, whereas we observe second order convergence for F_{F2}. These

Table 8: Evaluation of F_{S_1}, F_{S2}, F_{F1}, F_{F3} for ω_1 on various meshes.

	F_{S1}	F_{S2}	F_{S3}	F_{F1}	F_{F3}
$N = 2$	5.1111915e+19	1.5959672e−06	0	4.6850155e−06	1.1144903e−08
$N = 4$	5.1829593e+19	4.7395440e−07	0	1.2602854e−06	1.3157121e−09
$N = 8$	5.6563338e+19	1.3573087e−07	0	5.0983766e−07	2.4303798e−10
$N = 16$	6.8310894e+19	4.0580186e−08	0	2.4596621e−07	5.5167141e−11
	$F_{\Sigma 1}$	$F_{\Sigma 2}$			
$N = 2$	1.1276993e+17	3.2504259e+13			
$N = 4$	3.3814788e+16	1.3847004e+13			
$N = 8$	1.9770806e+16	9.7743548e+12			
$N = 16$	1.9632179e+16	8.6919628e+12			

rates of convergence are also shown in Figure 13. For the interface terms we do not measure an order of convergence.

The lack of convergence for the interface terms is better understood when studying the error as a function of space. The distribution of the error over the domain is shown in Figure 15 and Figure 14. From these figures, it becomes clear that the error is largest at the corners of the domain. This is not surprising, since the corners of the domain are expected to give rise to singularities of the solution. It also stands out that the error distribution of F_{S1} is large on the entire domain, with expected peaks in the corners. This could suggest a scaling problem of the variable $\boldsymbol{\sigma}$.

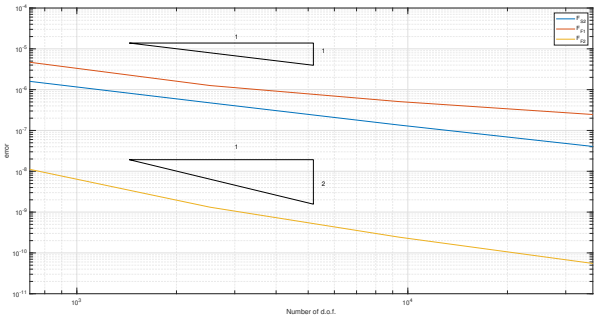

Figure 13: F_{S2}, F_{F1} and F_{F3} shown as function of the total number of d.o.f..

	order α_4	order α_8	order α_{16}
F_{S2}	1.7516	1.8040	1.7419
F_{F1}	1.8943	1.3056	1.0516
F_{F2}	3.0825	2.4366	2.1393
$F_{\Sigma 1}$	1.7377	0.7743	0.0102
F_{Σ_2}	1.2311	0.5025	0.1693

Table 9: Convergence order of F_{S2}, F_{F1}, F_{F2} and $F_{\Sigma 1}$.

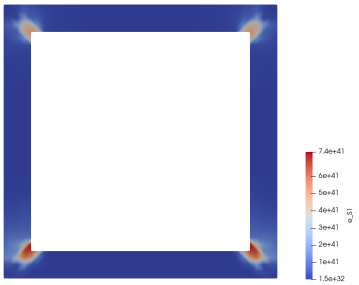

(a) F_{S1}.

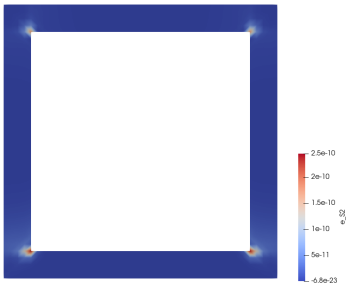

(b) F_{S2}.

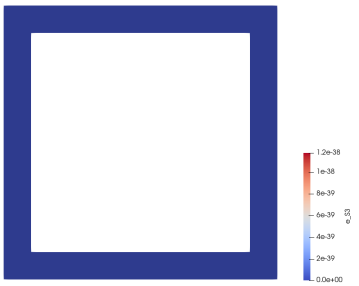

(c) F_{S3}.

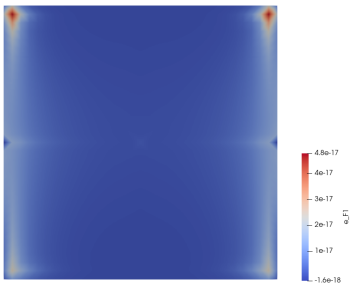

(d) F_{F1}.

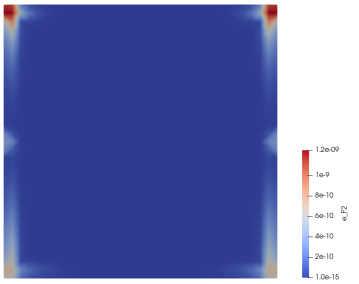

(e) F_{F2}.

Figure 14: Error distributions ofthe subfunctionals for ω_1 with $N = 4$.

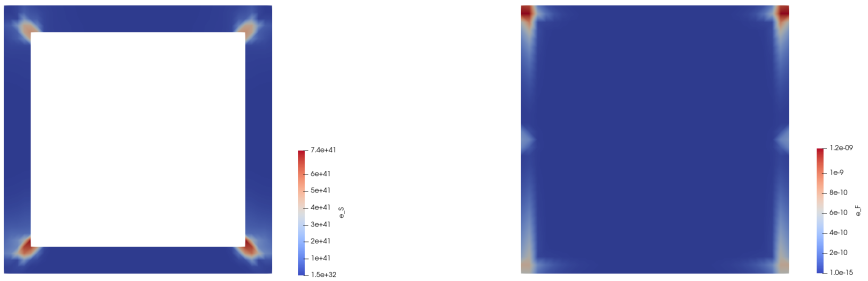

(a) F_S. (b) F_F.

Figure 15: Error distributions of the structure functional $F_S = F_{S1} + F_{S2} + F_{S3}$ and fluid functional $F_F = F_{F1} + F_{F2}$ for ω_1 for $N = 4$.

7 Conclusions and Outlook

7.1 Conclusions

The goal of this thesis was to investigate the least-squares finite element method for the fluid-structure interaction spectral problem. LSFEM has the advantage that it requires weaker restrictions as sufficient condition for existence and uniqueness in comparison with standard finite element methods. The only required condition is the norm-equivalence of the least-squares functional.
The fluid-structure interaction describes a linear elastic structure in contact with a fluid. The problem has been rewritten to a first order system, utilizing stress, displacement and vorticity in the elastic domain and pressure and the pressure gradient in the fluid domain. A finite element space was constructed using $H(div)$-conforming Raviart-Thomas elements in combination with piecewise polynomial functions. Standard approximation properties were provided.
Several least-squares formulations have been developed, giving rise to the corresponding variational formulations. A least-squares functional using L^2-norm residuals and weakly imposed boundary conditions has been analyzed further. The main theorem stated norm-equivalence of the LS functional. Norm-equivalence resulted in various advantageous properties of the (discrete) formulation, in particular, existence and uniqueness of the solution. The discrete formulation has been developed using the presented finite element spaces. As a consequence of norm-equivalence of the LS functional and the standard approximation properties an a priori error estimate was formulated. An a posteriori error estimate followed directly from the least-squares functional.
A numerical experiment describing a steel container filled with water was presented. In the numerical experiment we did not obtain any satisfactory results for the given computational setup. However, convergence of eigenvalues was observed in a simplified test case. Nonetheless, the physical implications of the eigenfunctions in this case remained unclear. Since this particular setup could not be compared with prior research, no decisive conclusions on the effectiveness of the LS method could be made.
Finally, the LS functional was applied as an a posteriori error estimate for different formulations of the fluid-structure interaction problem. Employing the LS functional as an a posteriori error estimate for the displacement/pressure formulation was only partially successful since not all terms of the LS functional converged with mesh refinements. Convergence for some parts of the LS functional could be demonstrated.

7.2 Outlook

With the numerical results not yielding the desired outcome, much progress can still be made when applying LSFEM to the fluid-structure interaction problem. Possible future research directions are summarized in the list provided below.

- **Scaling of the eigenproblem** As we have seen in Section 5.2, one of the computational problems may be the scaling of the problem. An obvious next step is to scale the LS functional, in the spirit of preconditioning, and investigate how scaling the problem can lead to a better conditioned problem.

- **Solving the source problem** The developed least-squares functional only describes the source problem with source term $\boldsymbol{f}_S$ and f_F. Only later, the variational formulation is extended to describe the eigenvalue problem. To better understand why

the numerical implementations of the eigenvalue problem do not converge, a simple setup of the source problem could be constructed.

- **Treatment of boundary terms** The LS functional analysed utilizes L^2 norms to capture the residual on the interface, instead of the fractional Sobolev norm. As mentioned in Section 4, this yields suboptimal results. Stevenson states in [23] that the fractional Sobolev norms can be replaced by equivalent efficiently computable quantities. Developing an LS functional utilizing these fractional Sobolev norms would therefore be of interest.

- **Implementations** While implementing the numerical experiment, we ran into some restrictions of the *FEniCS* platform. As mentioned in Section 5.1, inner products over the joint interface Σ cannot be easily constructed. Assembling the coupling matrices manually is prone to manual errors and can easily lead to mistakes. Furthermore, *FEniCS* could not handle inner products with Raviart-Thomas elements in all settings which was quite inconvenient and might be the cause of errors. To circumvent these problems, implementations using a different platform could be considered.

- **Sloshing modes** Once the numerical model delivers satisfactory results an interesting next step would be to expand the model with an open boundary of the fluid. This scenario includes sloshing movements which are common in physical examples.

References

[1] Alfredo Bermudez, Pablo Gamallo, Luis Hervella-Nieto, Rodolfo Rodriguez, and Duarte Santamarina. *Fluid–Structure Acoustic Interaction*, pages 253–286. Springer-Verlag, 01 2008.

[2] Alfredo Bermúdez and Rodolfo Rodríguez. Finite element computation of the vibration modes of a fluid—solid system. *Computer Methods in Applied Mechanics and Engineering*, 119(3):355–370, 1994.

[3] Markus Berndt, Thomas Manteuffel, and Steve McCormick. Local error estimates and adaptive refinement for first-order system least squares (fosls). *Electronic Transactions on Numerical Analysis*, 6:35–43, 12 1997.

[4] Fleurianne Bertrand and Daniele Boffi. First order least-squares formulations for eigenvalue problems. *IMA Journal of Numerical Analysis*, 42(2):1339–1363, 03 2021.

[5] Fleurianne Bertrand, Zhiqiang Cai, and Eun Young Park. Least-squares methods for elasticity and stokes equations with weakly imposed symmetry. *Computational Methods in Applied Mathematics*, 19(3):415–430, 2019.

[6] Fleurianne Bertrand, Lena Lambers, and Tim Ricken. Least squares finite element method for hepatic sinusoidal blood flow. *PAMM*, 20(1):e202000306, 2021.

[7] Pavel B. Bochev and Max D. Gunzburger. A least-squares finite element method for the navier-stokes equations. *Applied Mathematics Letters*, 6(2):27–30, 1993.

[8] Dietrich Braess. *Finite Elements: Theory, Fast Solvers, and Applications in Solid Mechanics*. Cambridge University Press, 3 edition, 2007.

[9] James H. Bramble, Tzanio V. Kolev, and Joseph E. Pasciak. The approximation of the maxwell eigenvalue problem using a least-squares method. *Mathematics of Computation*, 74(252):1575–1598, 2005.

[10] F. Brezzi and M. Fortin. *Mixed and Hybrid Finite Element Methods*. Springer series in computational mathematics. Springer-Verlag, 1991.

[11] Zhiqiang Cai and Gerhard Starke. First-order system least squares for the stress-displacement formulation: Linear elasticity. *SIAM Journal on Numerical Analysis*, 41, 11 2001.

[12] Carlos Conca, J Planchard, and Muthusamy Vanninathan. *Fluids and Periodic Structures*. Research in Applied Mathematics, 01 1995.

[13] Alexandre Ern and Jean-Luc Guermond. *Theory and Practice of Finite Elements*. Springer New York, NY, 2004.

[14] Lawrence C. Evans. *Partial Differential Equations*. American Mathematical Society, Providence, R.I., 2010.

[15] Max D. Gunzburger and Pavel B. Bochev. *Least-Squares Finite Element Methods*. Springer New York, NY, 2009.

[16] Bo-nan Jiang. *The least-squares finite element method: theory and applications in computational fluid dynamics and electromagnetics*. Springer Science & Business Media, 1998.

[17] Oliver Kayser-Herold and Hermann Matthies. Least squares finite element methods for fluid-structure interaction problems. *Computers & Structures*, 83:191–207, 01 2005.

[18] Oliver Kayser-Herold and Hermann Matthies. A unified least-squares formulation for fluid–structure interaction problems. *Computers & Structures*, 85(11):998–1011, 2007.

[19] Salim Meddahi and David Mora. Nonconforming mixed finite element approximation of a fluid-structure interaction spectral problem. *Discrete and Continuous Dynamical Systems - S*, 9(1):269–287, 2016.

[20] Salim Meddahi, David Mora, and Rodolfo Rodríguez. Finite element analysis for a pressure–stress formulation of a fluid–structure interaction spectral problem. *Computers & Mathematics with Applications*, 68(12, Part A):1733–1750, 2014.

[21] Steffen Münzenmaier and Gerhard Starke. First-order system least squares for coupled stokes—darcy flow. *SIAM Journal on Numerical Analysis*, 49(1/2):387–404, 2011.

[22] Roger Ohayon and Christian Soize. *Structural Acoustics and Vibration*. Academic Press, 1998.

[23] Rob P. Stevenson. First-order system least squares with inhomogeneous boundary conditions. *IMA Journal of Numerical Analysis*, 34(3):863–878, 10 2013.

A Nomenclature

Ω_S	structural domain
Ω_F	fluid domain
Γ_D	Dirichlet boundary
Γ_N	Neumann boundary
Σ	fluid structure interface
$\boldsymbol{\nu}_S$	outward normal on structural domain
$\boldsymbol{\nu}_F$	outward normal on fluid domain
$\mathcal{C}$	elasticity operator
$sym(\cdot),\ sk(\cdot)$	symmetric and skew-symmetric tensor parts
$\epsilon(\cdot)$	linearized strain tensor
$\boldsymbol{\delta}$	identity matrix
$\boldsymbol{\chi}$	skew-symmetric matrix
ρ_S	structure density
ρ_F	fluid density
c	acoustic speed
E, μ_P	elasticity modulus and Poisson ratio
λ, μ	Lamé coefficients
$\boldsymbol{f}_S$	source term
f_F	source term
$\boldsymbol{\sigma}$	structural stress tensor
$\boldsymbol{u}$	structural displacement vector
m	structural vorticity
π	fluid pressure gradient
p	fluid pressure